

GEOSYNTHETICS ENGINEERING, COMBINING TWO ENGINEERING DISCIPLINES

F. Tatsuoka¹

ABSTRACT: Geosynthetic-reinforced soil retaining walls (GRS RWs) with a stage-constructed full-height rigid facing are described to demonstrate the advantages of *Geosynthetics Engineering*. The paramount importance of due design and construction based on two engineering disciplines, *Material Engineering for Polymers* and *Geotechnical Engineering including Soil Mechanics*, in practice of *Geosynthetics Engineering* is emphasized by discussing on several issues of GRS walls. Based on laboratory test data and full-scale case histories, it is shown that, with polymer geosynthetic reinforcement as well as GRS walls, creep is not a degrading phenomenon and the tensile force activated in geosynthetic reinforcement arranged in properly designed and constructed GRS walls tends to decrease with time under static loading conditions: i.e., creep rupture failure of geosynthetic reinforcement is usually not a likely cause for collapse of GRS walls. It is shown that, when the backfill is well compacted and drained, geosynthetic reinforcement is not inferior to metal reinforcement in constructing soil structures allowing a limited amount of deformation. Some design issues are discussed based on these considerations.

Keywords: Creep reduction factor, Geosynthetics Engineering, Geosynthetic-reinforced soil retaining wall, Geotechnical Engineering, Geosynthetic reinforcement, Design shear strength of backfill

INTRODUCTION

The International Geosynthetics Society (the *IGS*) celebrates its 25th Anniversary this year, 2008. Reflecting on its history over the last quarter of a century, the *IGS*, as well as *Geosynthetics Engineering*, has been growing at a rapid rate. The main factor for this growth is, in *Civil Engineering (CE)* practice, *Geosynthetics Engineering* solutions are usually cost-effective (i.e., greater functionality at a lower cost; e.g., Giroud, 2008). Indeed, *Geosynthetics Engineering* meets the ultimate objective of *Civil Engineering*, i.e., more useful to society and the natural environment with greater functionality at a lower cost (Fig. 1).

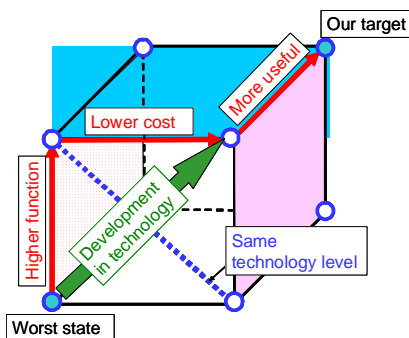


Fig. 1. Three requirements in *Civil Engineering* practice.

In this report, firstly geosynthetic-reinforced soil retaining walls (GRS RWs) with a stage-constructed full-height rigid facing as permanent important *CE* structures (not temporary structures) replacing conventional type RWs are described, as one of the most typical cost-effective solutions by *Geosynthetics Engineering*. This new technology typically meets the target of sustainable construction practice by a substantially lower amount of carbon dioxide (CO₂) emitted from the construction of soil retaining wall when compared to an equivalent conventional type steel-reinforced concrete soil retaining wall.

Secondly, it is addressed that *Geosynthetics Engineering* combines two engineering disciplines, *Material Engineering for Polymers* and *Geotechnical Engineering including Soil Mechanics*, and, if we ignore either of the two, we usually obtain wrong results, either overly conservative or overly un-conservative.

SOME JAPANESE EXPERIENCES WITH GRS RWs FOR LAST 20 YEARS

A Brief History

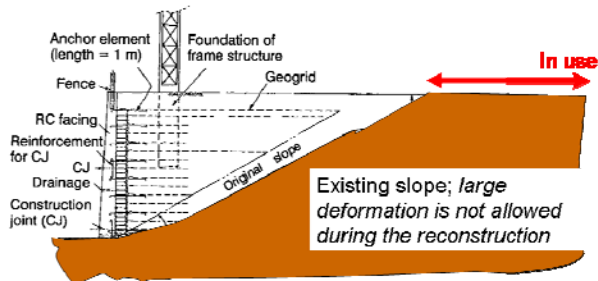
Geosynthetic-reinforced soil retaining wall (GRS RW) having a stage-constructed full-height rigid (FHR) facing is now the standard RW construction technology for

¹ Professor, Department of Civil Engineering, Tokyo University of Science, JAPAN. Email: tatsuoka@rs.noda.tus.ac.jp

railways (including those for bullet train lines) in Japan, in place of conventional RW technologies (Tatsuoka et al., 1997a, 2007a & b). A number of RWs of this type were also constructed for highways and other facilities. **Figs. 2** and **3** show typical initial large projects of GRS RWs having a FHR facing.



a)



b)



c-1)

Immediately after completion (1991)



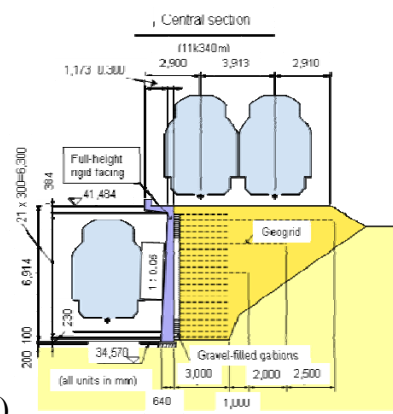
c-2)

15 years after construction (2006)

Fig. 2. Construction of Nagoya wall for a yard of bullet trains (Shinkan-Sen), average wall height = 5 m & total length = 930 m, during 1990-1991: the first large scale project: a) reconstruction of existing embankment slope; b) a typical cross-section; and c) typical views.



Fig. 3. Amagasaki wall in Hyogo Prefecture: the first large scale GRS RW supporting directly tracks for a very busy rapid railway (JR Kobe line), constructed during 1991-1992 under a severe space restriction; average wall height= 5 m & total length= 1,300 m.



a)



b)



c)

Fig. 4. A GRS RW having a FHR facing supporting one of the busiest urban rapid transits in Japan (Yamanote)

importance of this firm connection for a high wall stability is illustrated in **Fig. 8** (Tatsuoka, 1993).

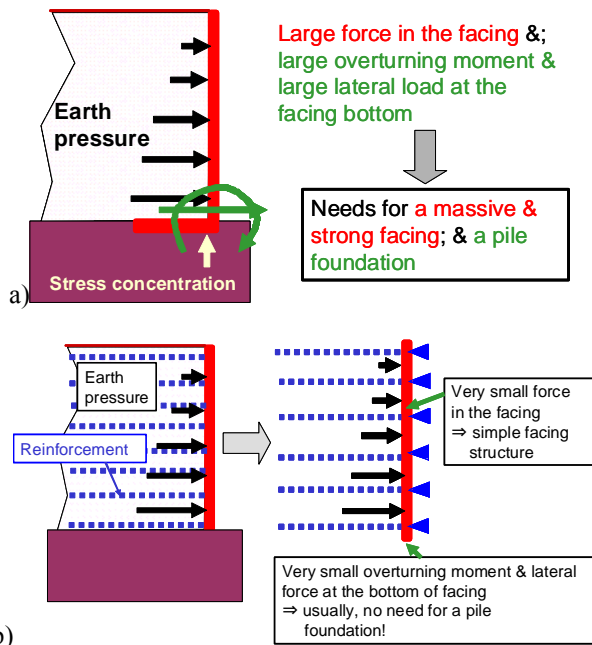


Fig. 9. a) Fundamental disadvantages with conventional type retaining walls as a cantilever structure; and b) advantages of GRS RW with a FHR facing as a continuous beam supported at many points with a small span (Tatsuoka et al., 1997a)

The firm connection between the reinforcement and the facing is particularly important to maintain a high wall stability under severe seismic loading conditions (Tatsuoka et al., 1998; Koseki et al., 2006). This is one of the major structural features of this new GRS RW system. That is, a conventional type RW is basically a cantilever structure that resists against the active earth pressure from the unreinforced backfill by the moment and lateral thrust force activated at its base (**Fig. 9a**). Therefore, large internal moment and shear force are mobilized inside the facing structure while large overturning moment and lateral thrust force develops at the base of the wall structure. A large stress concentration may develop at and immediately behind the toe on the base of the wall structure, which makes necessary the use of a pile foundation in usual cases. On the other hand, relatively large earth pressure, similar to the active earth pressure activated on the conventional RW, may be activated on the back of the FHR facing of GRS RW because of high connection strength between the reinforcement and the facing. This high earth pressure results in high confining pressure in the backfill, therefore high stiffness and strength of the backfill, which results in better performance than in the case without a firm connection between the reinforcement and the facing (**Fig. 8**). That is, a substantial reduction of earth pressure is not the target of this new GRS RW technology. As the FHR facing behaves as a continuous beam supported at a large number of levels with a small span, typically 30 cm (**Fig. 9b**), only small force is activated inside the FHR facing, which results in a much

simpler facing structure, and insignificant overturning moment and lateral thrust force activated at the bottom of facing, which makes unnecessary the use of a pile foundation unless the supporting ground is very soft and weak.

The second is the use of planar polymer geogrid reinforcement for cohesionless backfill to ensure good interlocking with the backfill and the use of a composite of non-woven and woven geotextiles for high water-content cohesive soils to facilitate both drainage and tensile reinforcement of the backfill, which makes possible the use of low-quality on-site soil as the backfill if necessary. The third is the use of relatively short reinforcement, which becomes possible by using: 1) planar geosynthetic reinforcement, which has a short anchorage length to resist against the tensile load equivalent equal to the tensile rupture strength of reinforcement; and 2) a FHR facing, which prevents the occurrence of local failure in the reinforced zone of the backfill by not allowing failure planes to pass through intermediate heights along the wall face. The advantages of the use of FHR facing become large in particular when the backfill is subjected to concentrated load on the top of the facing or immediately behind the wall face on the crest of the backfill.

The staged construction method (**Fig. 7**), which consists of the following steps, is another main feature of this GRS RW system:

- 1) A small foundation for the facing is constructed.
- 2) A full-height GRS wall with wrapped-around wall face is constructed by placing gravel-filled bags at the shoulder of each soil layer.
- 3) A thin (i.e., 30 cm or more in the thickness) lightly steel-reinforced concrete facing (i.e., a FHR facing) is constructed by casting-in-place fresh concrete directly on the wall face covered with a wrapped-around geogrid after the major part of ultimate deformation of the backfill and the subsoil layer beneath the wall has taken place. A good connection can be made between the RC facing and the main body of the wall by placing fresh concrete directly on the geogrid-covered wall face.

By this staged construction method, the connection between the reinforcement and the facing is not damaged by differential settlement between the FHR facing and the backfill during wall construction, while sufficient tensile force is mobilized in the reinforcement during construction. Then, construction of walls on relatively compressible subsoil becomes possible. These two advantages cannot be expected when a FHR facing is erected and propped before the start of embankment. In that case, the connection between the reinforcement and the backfill may be damaged by differential settlement between the reinforcement and the backfill by the deformation of backfill and supporting ground, and tensile force is mobilized in the geosynthetic reinforcement only after the propping is removed after the wall is completed. This procedure may result in

uncontrolled and relatively large lateral outward displacements of the facing that may last for a long duration after the wall is opened to service.

A great number of case histories of GRS RW having a stage-constructed FHR facing until today (Fig. 5) have shown that this type of GRS RW is much more cost-effective (i.e., much lower construction cost, a much higher construction speed and the use of much lighter construction machines, therefore a much less total emission of CO₂) than conventional type RWs. It is also important to note that the performance of this new type RWs is equivalent to, or even better than, conventional type soil RWs.

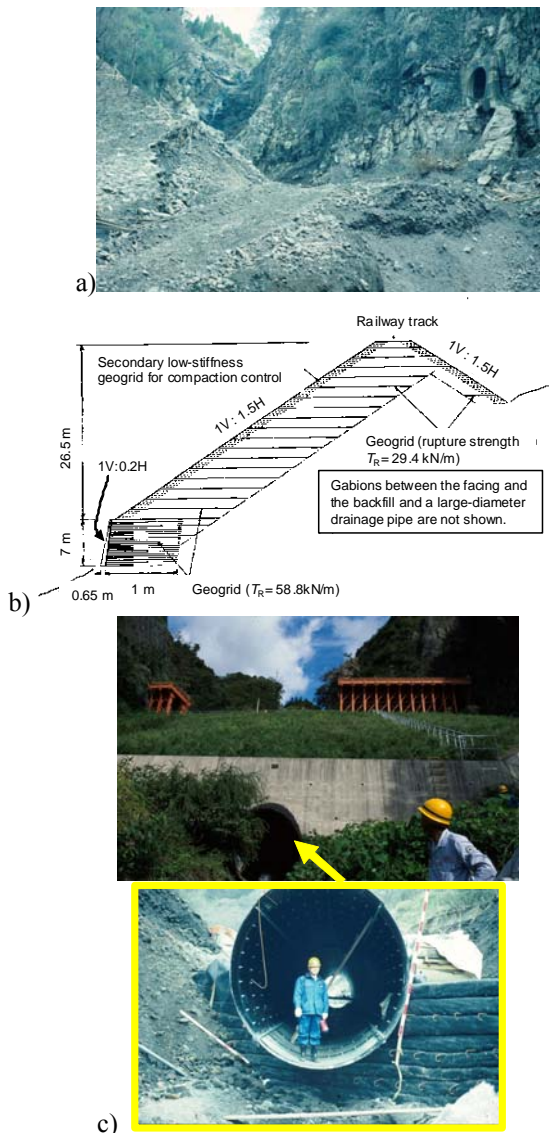


Fig. 10 A typical section of railway embankment damaged by rainfall in 1989 and reconstructed in 1991: a) before reconstruction; b) reconstructed cross-section; and c) after reconstruction (Tatsuoka et al., 1997b; 2007a&b).

GRS-RWs for Reconstruction

Previously, most of soil structures (i.e., sloped embankments and RWs) collapsed by heavy rainfalls, floodings and earthquakes were reconstructed to respective original type soil structures, despite that they are not cost-effective with rather low resistance against these natural disasters. Recently, this new type GRS-RWs were constructed not only as new RWs but also to reconstruct embankments and conventional type RWs that collapsed by earthquakes and flooding.



Fig. 11. Gravity type RW without a pile foundation at Ishiyagawa that collapsed during the 1995 Kobe Earthquake (Tatsuoka et al., 1996, 1997a & b)

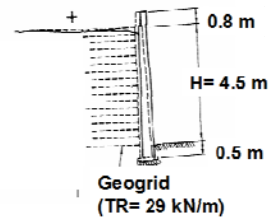


Fig. 12. A GRS RW having a FHR facing at Tanata, Japan: a) immediately after wall completion; and b) immediately after the 1995 Kobe Earthquake (Tatsuoka et al., 1996, 1997a & b)

In the beginning of 1990's, reconstruction of railway embankments that collapsed by flooding to

embankments having geosynthetic-reinforced steep slopes or GRS RWs having a stage-constructed FHR facing or their combination started. **Fig. 10** shows a typical case of the above (Tatsuoka et al., 1997a; 2007b). This reconstruction method was employed also in other similar cases by subsequent events of flooding. **Fig. 11** shows typical damage to a conventional type RW during the 1995 Hyogo-ken Nambu Earthquake (i.e., Kobe Earthquake) (Tatsuoka et al., 1996, 1997a & b). In comparison, GRS-RWs having a stage-constructed FHR facing behaved very satisfactorily. **Fig. 12** shows a GRS RW with a stage-constructed FHR facing at Tanata that performed very well during the 1995 Kobe Earthquake.



Fig. 13 a) Collapse of a gravity type (leaning type) RW during the 1995 Kobe Earthquake; and b) reconstructed GRS-RW having a stage-constructed FHR facing (Tatsuoka et al., 1996, 1997a & b)

A number of conventional type railway RWs that collapsed during this earthquake were re-constructed to GRS RWs having a stage-constructed FHR facing (**Fig. 13**). After the 1995 Kobe Earthquake, reconstruction of gentle slopes of embankment and conventional RWs that collapsed by earthquakes to geosynthetic-reinforced steep slopes or GRS RWs having a stage-constructed FHR facing or their combination is becoming more popular (Tatsuoka et al., 1997a & b; 2007a & b; Koseki et al., 2006; 2007). **Fig. 14** shows reconstruction of one of the three railway embankments that totally failed during the 2004 Niigata-ken Chuetsu Earthquake to GRS RWs having a stage-constructed FHR facing. In this case, this new type GRS RW was chosen because of not only much lower construction cost and much higher stability (in particular for soil structures on a steep slope) but also a much shorter construction period because of significantly reduced earthwork when compared to reconstruction to the original embankments. The construction period is also much shorter than bridge type structures. During this earthquake, road embankments collapsed at numerous places in mountainous areas and many of them were reconstructed to GRS RWs or

embankments having geosynthetic-reinforced steep slopes (Koseki et al., 2006).

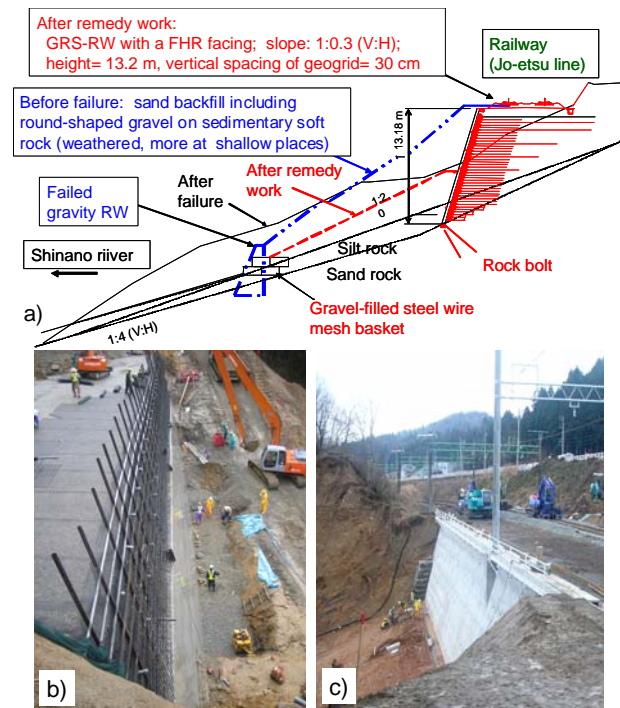


Fig.14. Railway embankment that collapsed during the 2004 Niigata-ken Chuetsu Earthquake and its reconstruction to a GRS RW having a FHR facing: a) cross-sections before and after failure and after reconstruction; b) the wall during reconstruction; and c) the completed wall (Morishima et al., 2005).

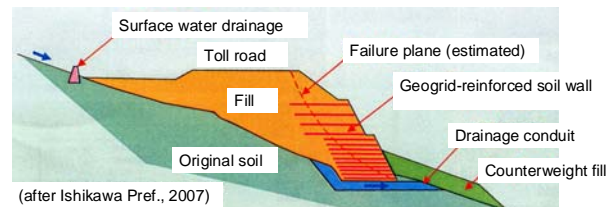


Fig. 15. Schematic diagram showing reconstruction to GRS walls of embankments damaged by the 2007 Noto hanto Earthquake (Koseki et al., 2007).

More recently, the March 25, 2007 Noto-Hanto Earthquake caused severe damage to embankments of Noto Toll Road, which was opened in 1978 to 1980. The north part of this road runs through a mountainous area for a length of 27 km. The damage concentrated into this part, where eleven high embankments filling valleys extensively collapsed (Koseki et al., 2007). As shown in **Fig. 15**, the collapsed embankments were basically reconstructed to embankments having GRS RWs while ensuring the drainage of ground and surface water. The on-site soil that had originally been part of the collapsed embankment was re-used after lime-treatment for the construction of the upper fill.

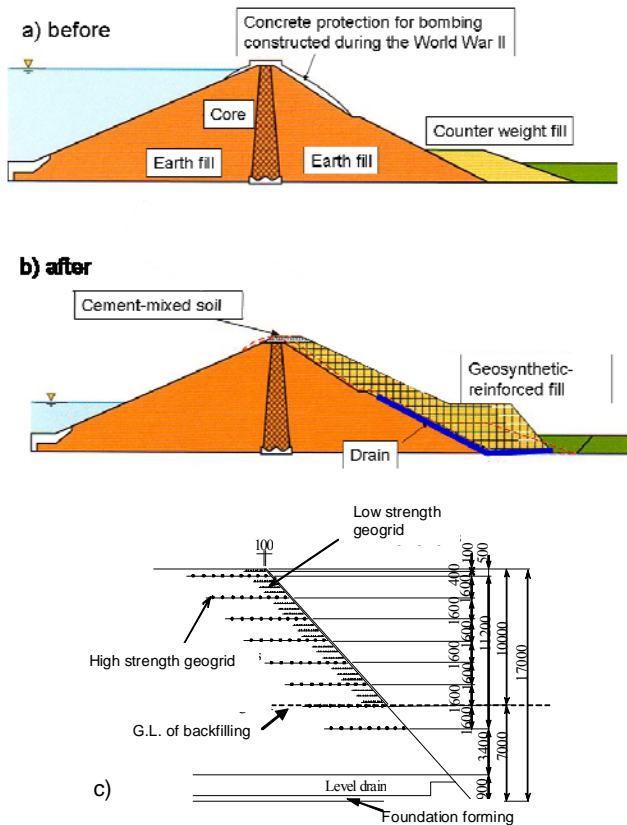


Fig. 16. Shimo-Murayama dam in Tokyo: a) & b) dam before and after rehabilitation; and c) geogrid-reinforced counter-weight fill (Maruyama et al., 2006)

The GRS wall technology was also used to rehabilitate an old earth dam, having a crest length of 587 m and a height of 33.6 m, in the north of Tokyo (Fig. 16). When constructed about 80 years ago, this earth dam was the largest one in Japan. The reservoir is exclusively for water supply in Tokyo, which will become extremely important in supplying water at the time of disaster, including seismic one, because of its ability of sending raw water in gravity flow to several water purification plants on the downstream. A 17 m-high counter-weight fill having a 1:1 steep slope was constructed on the down-stream slope of the dam aiming at a substantial increase in the seismic stability of the dam. This rehabilitation removed a possibility of vast disaster to a heavily populated residential area that had developed recent years in front of the dam. Due to a severe space restriction, the slope of the counter-weight fill was made very steep by being reinforced with layers of HDPE geogrid installed over a total area of 28,500 m² in the fill.

Summary

A great number of successful case histories, as described above, have validated the advantages of the GRS RWs having a stage-constructed FHR facing as well as GRS walls in general. In particular, when compared to two decades ago, this type of GRS RWs are much more widely accepted as a relevant technology to

construct new RWs and to reconstruct embankments and conventional RWs that have collapsed by floodings and earthquakes. The structural advantages of using a FHR become more significant when concentrated load is activated on the top of the facing or immediately behind the facing on the backfill crest. The most recently proposed application is to construct GRS RWs having a stage-constructed FHR facing as bridge abutments of an integral bridge (i.e., the GRS integral bridge, Fig. 17; Aizawa et al., 2007; Hirakawa et al., 2007; Tatsuoka et al., 2007c; 2008b & c).

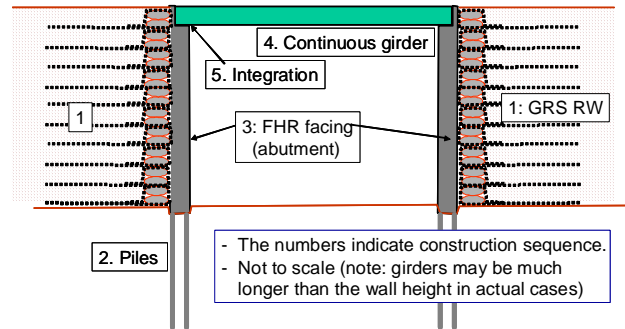


Fig. 17. GRS integral bridge, the backfill reinforced with geosynthetic reinforcement connected to the facing (Tatsuoka et al., 2007c, 2008b & c)

IMPORTANCE OF INTEGRATION OF TWO ENGINEERING DISCIPLINES

Polymer Reinforcement, Too Extensible and May Rupture by Creep ?

Geosynthetics Engineering is unique in that it combines two engineering disciplines, *Material Engineering*, specific to polymer materials, and *Geotechnical Engineering*, including Soil Mechanics. The importance of combining these two engineering disciplines is obvious in the soil-reinforcing technology, as described above. It seems, however, that there are some serious misunderstandings about the geosynthetic-reinforcing technology resulting from: a) some basic misunderstanding in the respective disciplines; and/or b) ignoring *Geotechnical Engineering* discipline in *Geosynthetics Engineering* practice. Typical of the above is that polymer geosynthetic reinforcement is often called extensible reinforcement, while metal (usually steel) reinforcement is often called inextensible reinforcement. This definition may be relevant when comparing the stiffness values of these two types of reinforcement alone (i.e., when they are extended in-air or in-isolation). Unfortunately, this definition often leads to the following wrong impressions or misunderstandings by civil engineers who may control construction projects but are not specialized in *Geosynthetics Engineering*:

- 1) Creep rupture failure of polymer geosynthetic reinforcement is one of the major causes for collapse of GRS structures.

2) Geosynthetic reinforcement is too extensible and therefore inferior to metal reinforcement in constructing soil structures (i.e., steep slopes and soil RWs) allowing a limited amount of deformation. The main problem is that these wrong notions are still popular and they often restrain the use of GRS wall structures where and when they should be adopted. In the following, this issue is analyzed by discussing on; firstly in-air (i.e., in-isolation) behaviour of geosynthetic reinforcement in the field of *Material Engineering of Polymers*; secondly in-soil behaviour of geosynthetic-reinforcement combining *Material Engineering of Polymers* and *Soil Mechanics*; and thirdly behaviour of geosynthetic-reinforced soil in the field combining *Material Engineering of Polymers* and *Geotechnical Engineering*.

In-Air Behaviour of Geosynthetic Reinforcement

In this section, it is shown that, with in-air geosynthetic reinforcement in tension, creep is not a degrading phenomenon. That is, the strength at the same strain rate of polymer geosynthetic does not decrease with an increase in the period of creep loading applied in the pre-peak regime unless time-dependent chemical and/or biological deterioration takes place. The changes in the micro-structure of reinforcement that take place during a creep process are not different from those that take place during continuous monotonic loading (ML).

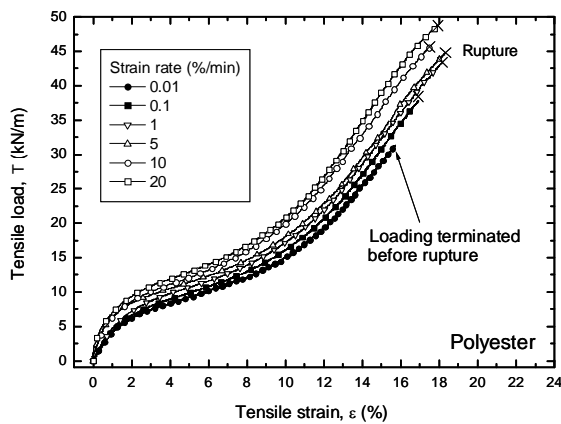


Fig. 18. Dependency of tensile load-strain behaviour on strain rate, a PET geogrid (Hirakawa et al., 2003).

Current popular method to determine the design rupture strength: The use of polymer geosynthetic reinforcement has become popular in the construction of reinforced soil structures, recently perhaps more than the use of metal strip/grid reinforcement. When reinforced with metal reinforcement, the vertical and horizontal spacing is usually large, say 1 m, accounting for its relatively high stiffness and strength. This arrangement results in a less contact area with the backfill, which may result into a pull-out failure (e.g., Lee et al., 1994). Another potential serious problem is a low bond stress and a danger of accelerated rusting when arranged in high water content clayey backfill. On the other hand, polymer geosynthetic reinforcement having a planar

global form is arranged in the backfill at a relatively small vertical spacing, say 30 cm, accounting for its relatively low stiffness and strength. As a result, the deformation of GRS structures that takes place by the end of construction may become larger than that of metal-reinforced soil structures under otherwise the same conditions (e.g., Christopher et al., 1994). However, the deformation of reinforced soil structures by the end of construction, before opened to service, is usually not a serious engineering problem unless it is too large. Rather, 1) excessive residual deformation of structure due to viscous deformation of backfill and reinforcement that would take place after having been opened to service (as discussed later); and 2) long-term material degradation and also an associated possibility of creep rupture of reinforcement are among concerned potential serious problems.

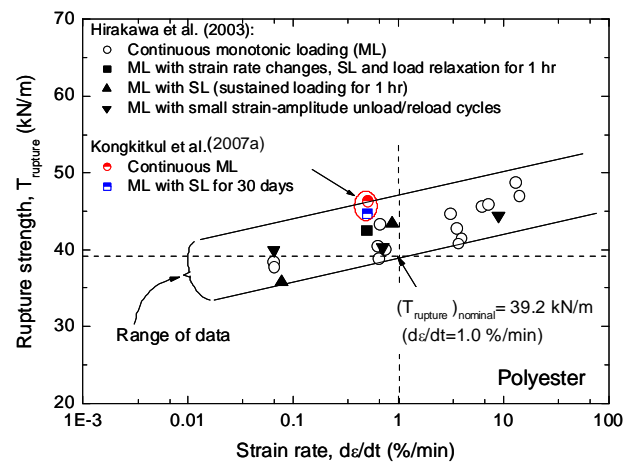


Fig. 19. Dependency of rupture strength on the strain rate at rupture, a PET grid (ML: monotonic loading; SL: sustained loading; and LR: load relaxation) (Hirakawa et al., 2004).

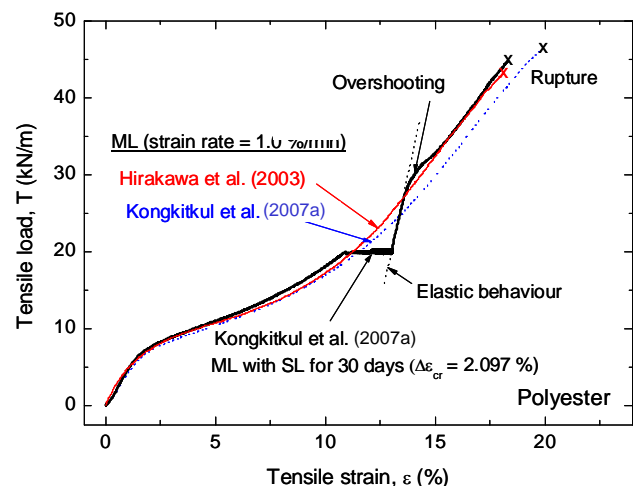


Fig. 20. Comparison of tensile load - strain relations from ML tests with and without creep loading for 30 days at an intermediate load level, a PET geogrid (Kongkitkul et al., 2007a).

Related to the two potential problems cited above, the tensile deformation and strength characteristics of polymer geosynthetic reinforcement are more-or-less rate-dependent due to its viscous property (e.g., Bush, 1986; Bathurst & Cai, 1994; Min et al., 1995; Leshchinsky et al., 1997; Zornberg & Kavazanjian, 2002; Zornberg et al., 2004; Hirakawa et al., 2003; Kongkitkul et al., 2004, 2007a & b; Kongkitkul & Tatsuoka, 2007; Tatsuoka et al., 2004; Shinoda & Bathurst, 2004a & b, Kazimierowicz-Frankowska, 2005; Bueno et al., 2005; and Liu & Ling, 2006). **Fig. 18** shows results from ML tensile tests on a PET geogrid at different strain rates, typically showing the above. **Fig. 19** shows that the rupture strength increases with an increase in the strain rate at rupture. Creep deformation is defined as the deformation that takes place due to material viscosity at constant load. **Fig. 20** shows a typical tensile loading test on the same PET geogrid as used in the tests described in Fig. 18. In one of the tests, creep loading was performed for 30 days during otherwise ML at a constant strain rate, and the result is compared with those from two continuous ML tests. The rupture strengths from the two ML tests are slightly different due to the use of different samples from different batches obtained four years apart. The rupture strengths from the two tests using new samples (one continuous ML and one ML with creep loading, shown in Fig. 20) are plotted in Fig. 19. They are slightly larger than those obtained using old samples.

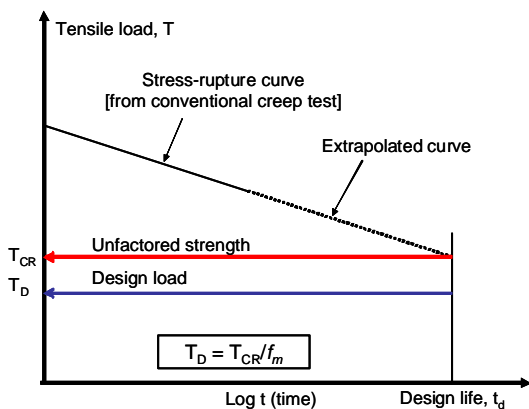


Fig. 21. Conventional creep rupture curve, after Greenwood (1994)

In the current design procedure, the design tensile strength at the end of a specified design life time (T_d) of a given polymer geosynthetic reinforcement type is obtained by reducing a short-term tensile strength obtained from a relatively fast continuous ML test (T_{ult}) using a relatively large creep reduction factor. The creep reduction factor is obtained based on the so-called “stress-rupture curve” (i.e., the relationship between the sustained constant tensile load and the logarithm of the period until creep rupture since the start of sustained loading, SL), as illustrated in **Fig. 21** (Greenwood, 1994). The stress-rupture curve is obtained by performing a set of conventional creep rupture tests. The period until creep rupture becomes shorter with an increase in the

load level. As the conventional creep rupture tests are significantly time-consuming, Thornton et al. (1998) proposed a method called “Stepped Isothermal Method (SIM)” to reduce the time to rupture by step increasing the temperature of environment surrounding on the test specimen.

More specifically, aiming at preventing the failure of geosynthetic-reinforced soil structure due to tensile rupture of geosynthetic reinforcement as a result of excessive creep deformation, which may have been accelerated by material degradation, FHWA (2001) specified that the long-term design tensile strength (i.e., the design applied load, T_d), of given geosynthetic reinforcement is obtained by separately accounting for the negative effects of several influencing factors on the tensile strength as:

$$T_d = T_{ult} / \{RF_{CR} \cdot RF_D \cdot RF_{ID} \cdot (F_s)_{overall}\} \quad (1)$$

where:

T_{ult} is the ultimate tensile strength based on minimum average role value (MARV);

RF_{ID} is the installation damage factor (typically 1.05 – 3.0);

RF_D is the durability reduction factor (typically 1.1 – 2.0) to account for long-term chemical and/or biological degradation effects;

RF_{CR} is the creep reduction factor (> 1.0) to avoid creep rupture until the end of service life; and

$(F_s)_{overall}$ is the overall factor of safety to account for uncertainties in the geometry of the structure, fill properties, and external applied loads. A minimum $(F_s)_{overall}$ of 1.5 has been typically used.

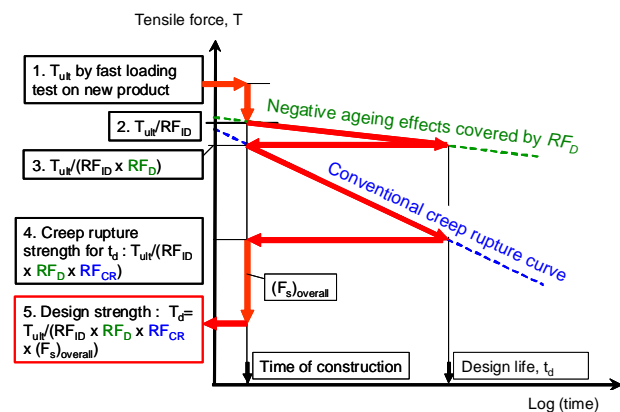


Fig. 22. Method popularly used to obtain the long-term design tensile strength of a given geosynthetic reinforcement (Tatsuoka et al., 2004, 2006, Kongkitkul et al., 2007b & d)

Fig. 22 illustrates the design procedure according to Eq. 1, which consists of steps 1 to 5:

1. T_{ult} is obtained from relevant fast tensile loading tests on virgin specimens (e.g., ASTM D4595).
2. RF_{ID} is estimated for a given condition of construction and then applied to obtain T_{ult}/RF_{ID} .

3. RF_D for a given design life is estimated and then additionally applied to obtain $T_{ult}/(RF_D \cdot RF_{ID})$.
4. RF_{CR} for the design life is obtained based on a given conventional creep rupture curve. The value of RF_{CR} is different among different types of polymer and different national design standards: e.g., 4.0 – 5.0 for polypropylene (PP) and 2.6 – 5.0 for high-density polyethylene (HDPE) according to FHWA (2001). Then, RF_{CR} is additionally applied to obtain $T_{ult}/(RF_{CR} \cdot RF_D \cdot RF_{ID})$.
5. $(F_s)_{overall}$ is finally applied to obtain the long-term design tensile strength, T_d (Eq. 1).

Despite its very popular use, this method (Eq. 1) has the following three major drawbacks, which jointly may result in over-conservative design.

Firstly, the original objective of this design procedure is to remove the possibility of creep rupture failure of geosynthetic reinforcement during service time and its implication is that, as the time to creep tensile rupture increases with a decrease in the sustained load, smaller design strength should be used for a longer design life time. That is, the creep rupture curve is not a diagram of reduction in strength against time. However, when following this current design procedure, the design tensile strength always decreases with an increase in the design life time, and therefore, this curve may appear to be a diagram of reduction in strength against time. This may lead to a wrong notion that creep is a degrading phenomenon. It may be seen from Fig. 20, however, that, unless the strength and deformation characteristics of a given polymer geosynthetic reinforcement chemically and/or biologically degrades with time, the tensile strength for the same loading condition (e.g., ML at the same constant strain rate) does not decrease by intermediate creep loading for some long time (i.e., 30 days in this case). It may be seen from Fig. 19 that the rupture strength is basically a function of strain rate at rupture, while pre-rupture creep deformation and other arbitrary loading histories do not affect the tensile rupture strength. Many other similar data for other geosynthetic reinforcement types can be found in the literature (Bernardi & Paulson, 1997; Hirai & Yatsu, 2000; Voskamp et al., 2001; Greenwood et al. 2001; Hirakawa et al., 2003; Kongkitkul et al., 2004, 2007a; Onodera et al., 2004; Tatsuoka et al., 2004; Shinoda & Bathurst, 2004a & b).

Based on the fact that creep is not a degrading phenomenon, Greenwood et al. (2001), Tatsuoka et al. (2004, 2006) and Kongkitkul et al. (2007b) proposed a new design procedure in which the residual or available strength of a polymer geosynthetic reinforcement is a function of strain rate at rupture, not elapsed time (Fig. 23). Lines 1, 2 and 3 indicate three different residual strengths for three different strain rates at rupture (i.e., the strength that are available when loaded at respective strain rates after having been subjected to constant load equal to the unfactored strength). That is, unless the material property degrades with time by chemical and/or

biological effects, the original strength of a geosynthetic reinforcement (for a given strain rate at rupture) is maintained until late in its service life. This new proposal (Fig. 23) is no doubt much more relevant than the conventional method (Fig. 22) in the case of seismic design of GRS structures that are subjected to seismic load after some long service period at constant boundary load. This issue is discussed again later.

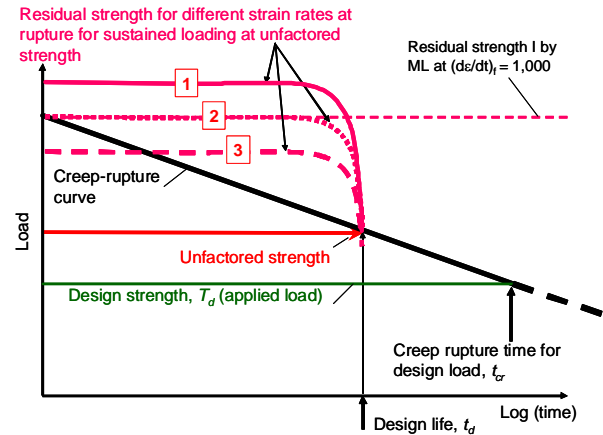


Fig. 23. Effects of strain rate at rupture on residual strength, after Tatsuoka et al. (2004)

Secondly, Eq. 1 assumes that the long-term sustained loading (SL) (i.e., creep loading) starts after the material has fully degraded by a factor of $1/RF_D$ due to the use in the backfill for the design life: i.e., SL starts after having backed from the future. In actuality, creep deformation and material degradation take place simultaneously during the design life. Therefore, it is more-or-less conservative to determine the design rupture strength by separately taking into account the creep reduction factor, RF_{CR} , and the durability reduction factor, RF_D , based on Eq. 1.

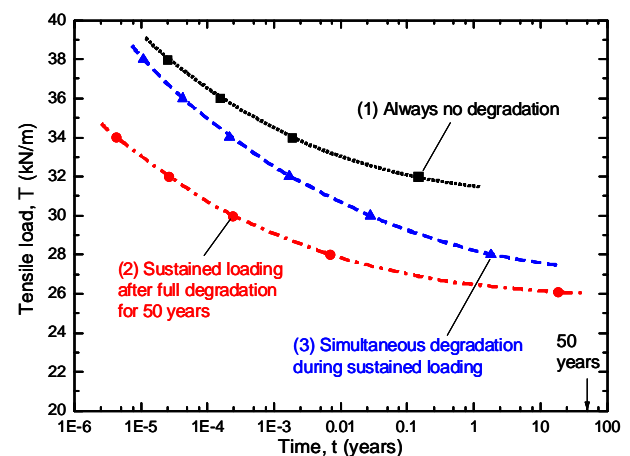


Fig. 24. Creep rupture curves obtained by simulation under three different degradation conditions (Kongkitkul et al., 2007b)

Fig. 24 compares the following three creep rupture curves of typical polymer geosynthetic reinforcement under typical conditions obtained by simulations

introducing material degradation effects into a non-linear three-component rheology model (Kongkitkul et al., 2007b), which is explained later:

- 1) when the material does not degrade at all during the design life;
- 2) when SL starts after full material degradation has taken place for the service life and there is no degradation after the start of SL (i.e., Eq. 1 & Fig. 22); and
- 3) when material degradation takes place simultaneously during SL which lasts for the design life (i.e., the actual case).

These simulations did not aim at analysis of the behaviour of any specific geosynthetic reinforcement type, but the simulations were designed to represent the behaviour of typical geosynthetic reinforcement types. It may be seen that case 2 (i.e., Eq. 1) underestimates the creep rupture strength under realistic conditions (i.e., case 3). That is, it is more-or-less conservative to determine the design rupture strength based on Eq. 1.

Thirdly, Eq. 1 assumes that the tensile load working in polymer geosynthetic reinforcement is kept constant under long-term fixed static boundary conditions during the design life. However, this is usually a conservative assumption, perhaps overly, as discussed later.

Due to these three drawbacks, the conventional design method (Eq. 1) is likely to be largely conservative, definitely with GRS walls that are designed and constructed as permanent critical structures having a sufficiently high seismic stability.

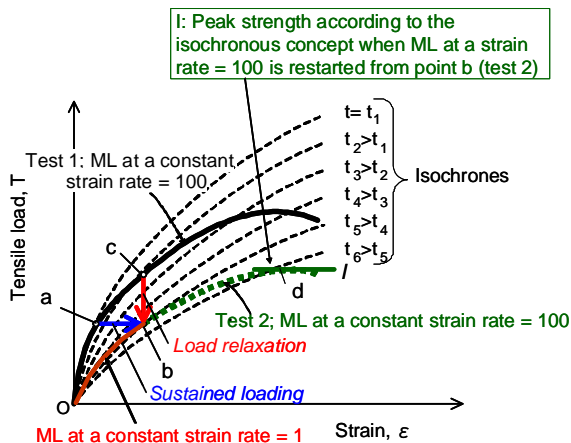


Fig. 25. Responses of geosynthetic reinforcement to different loading histories according to Isochronous concept (see Fig. 27a for test 2).

Isochronous concept: The misunderstandings about the current design methodology (Eq. 1) explained above are implicitly and explicitly linked to the isochronous concept. This concept states that “the present tensile load acting in given polymer geosynthetic reinforcement is a unique function of instantaneous strain and elapsed time since the start of loading”. According to the isochronous concept, the following trends of behaviour should be obtained (Fig. 25): i.e., after the same elapsed

time ($t = t_5$) since the start of loading, the same stress-strain state (point **b**) is reached by: 1) fast loading until point **a**, followed by SL until point **b**; 2) fast loading until point **c**, followed by load relaxation until point **b**; and 3) continuous slow ML until point **b**. It is difficult to show that the isochronous theory is wrong only based on results from a set of ML tests performed at different constant strain rates, as shown in Fig. 18. In Fig. 26, the tensile load–tensile strain curves from three continuous ML tests performed at three different constant strain rates, denoted as 1, 10, and 100, are depicted. It is possible to construct contours of equal elapsed time (i.e., isochrones) based on these test results. Then, one may consider that the stress-strain curve is controlled by time.

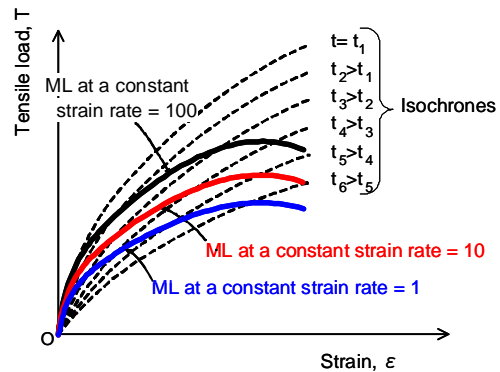


Fig. 26. Interpretation of results from ML at different constant strain rates by Isochronous concept.

Hirakawa et al. (2003), Kongkitkul & Tatsuoka (2007), Kongkitkul et al. (2004, 2007a & b) and Tatsuoka et al. (2004) showed that the isochronous concept is not able to predict and explain the load-strain behaviour of given geosynthetic reinforcement for general arbitrary loading histories. The relevance of the isochronous theory can be examined easily by analysing load-strain behaviour after ML is restarted at the original constant strain rate following a SL staged performed during otherwise ML at a constant strain rate. That is, referring to Fig. 27a, suppose that the following three tensile tests are performed:

Test 1: ML continues at a high strain rate (= 100) towards ultimate failure.

Test 2: ML continues at a high strain rate until point **a** (at a relatively high load level), from which SL starts and ends at point **b**. From point **b**, ML restarts at the original high strain rate (= 100) towards rupture.

Test 3: The loading history is similar to that of test 2, except that the load level during SL is very low.

As shown in Fig. 25, according to the isochronous model, when fast ML at a strain rate equal to 100 restarts from point **b** in test 2, the load-strain relation should be located below the isochrone for $t = t_5$, passing through point **b**, since we cannot go back to the past. Then, the rupture strength (at point **d**) obtained by test 2 becomes smaller than the one obtained by test 1 (i.e., continuous fast ML until rupture). The rupture strength decreases more with an increase in the period of SL **a-b**. This indeed implies that creep is a degrading phenomenon. Furthermore, as shown in Fig. 27b, the same amount of

strength reduction by SL as test 2 is observed in test 3, despite that the sustained load at stage *e-f* is substantially lower than the one at stage *a-b* in test 2. **Fig. 27c** compares the load-strain curves from tests 2 and 3.

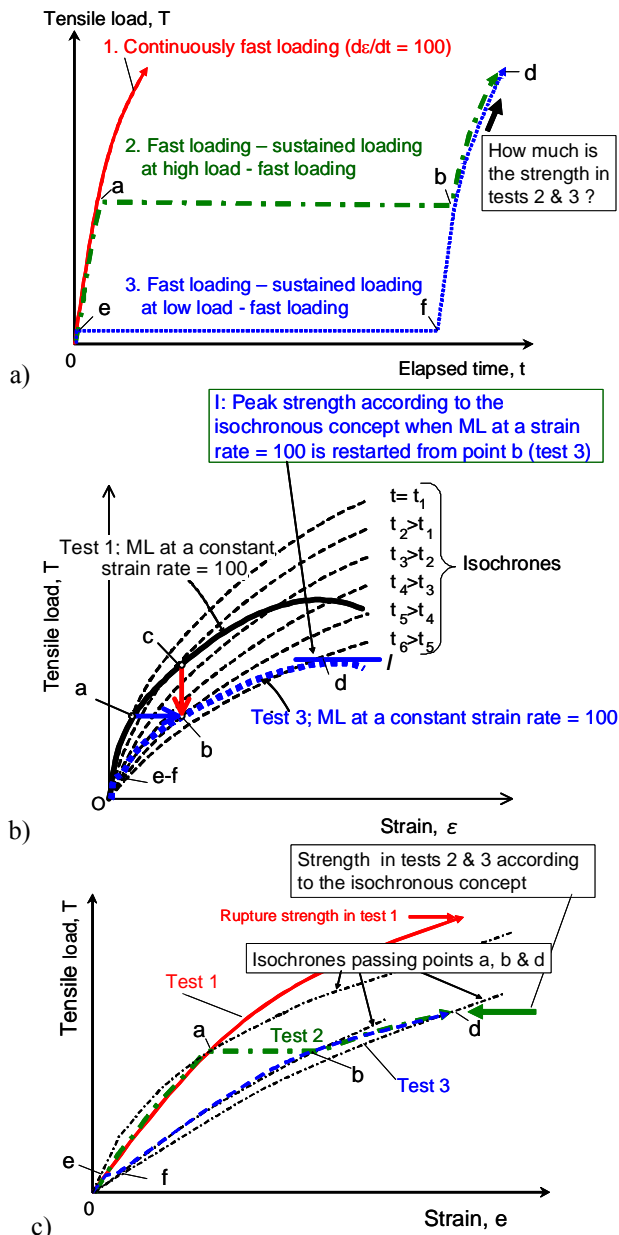


Fig. 27. a) Loading histories designed to examine the relevance of Isochronous Concept; and b) & c) responses of geosynthetic reinforcement to different loading histories according to Isochronous Concept.

On the other hand, **Fig. 28a** illustrates the actual behaviour of geosynthetic reinforcement, as presented in Fig. 20. That is, when fast ML at a strain rate equal to 100 restarts at point *b'* in test 2, the load-strain relation first shows very stiff behaviour, close to the elastic one. The stiff behaviour continues until rejoining the relation from test 1 (i.e., continuous fast ML until rupture), without overshooting with most types of polymer geosynthetic reinforcement (Hirakawa et al., 2003; Kongkitkul et al., 2004). Therefore, the rupture strength

obtained from test 2 is essentially the same as the one from test 1, irrespective of the period of SL *a-b'*. The same trend of behaviour after SL as in test 2 is observed in test 3 (**Fig. 28b**). **Fig. 28c** compares the load - strain curves from tests 2 and 3. Indeed, Isochronous Concept is theoretically incorrect and practically misleading. As illustrated in Fig. 28a, the same stress-strain state (point *b*) is not reached after the same elapsed time since the start of loading by the following three loading histories: 1) fast loading until point *a*, followed by SL (until point *b'*); 2) fast loading until point *c*, followed by load relaxation (until point *b*); and 3) continuous slow ML (until point *b''*).

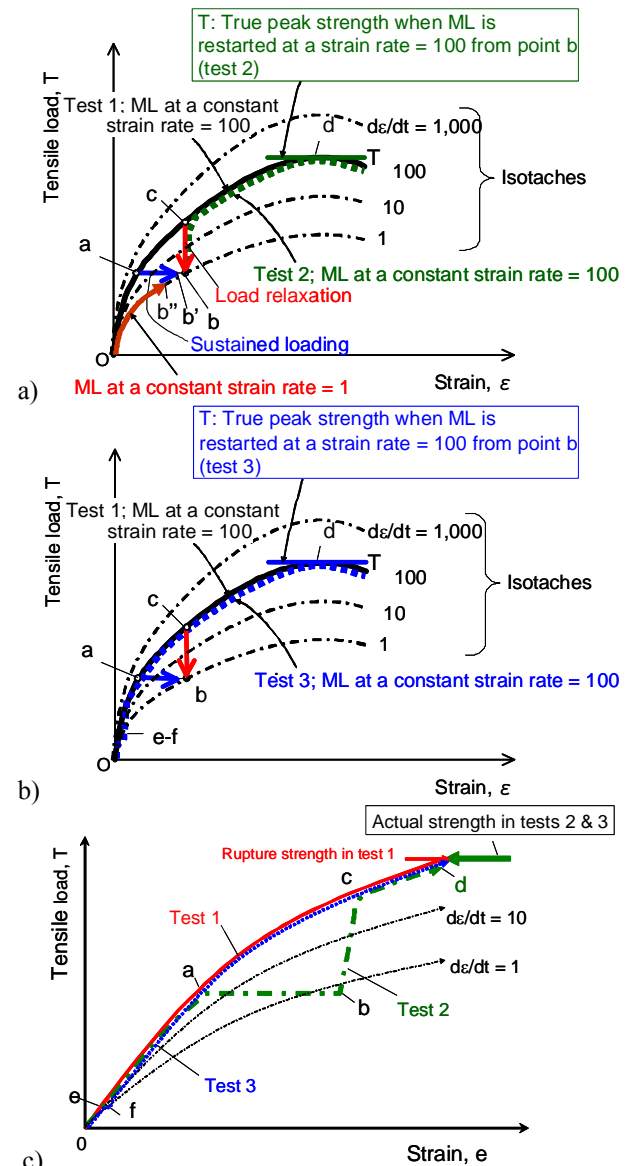


Fig. 28. Actual responses of geosynthetic reinforcement to different loading histories (in the case of isotach viscous property).

Non-linear three-component model: We need a relevant constitutive model of polymer geosynthetic reinforcement to infer loads in reinforcement from measured strains, as we cannot measure loads directly.

Only with elastic materials, we can uniquely determine the stress state from strain states without referring to previous loading histories if the initial unstressed state is known. The viscous properties of granular materials, which are used as the backfill for most GRS structures, have been studied extensively and a non-linear three-component elasto-viscoplastic model (Fig. 29a) was proposed (e.g., Di Benedetto et al., 2002, 2005; Tatsuoka et al., 2000, 2001, 2002, 2008a; Tatsuoka, 2004, 2007; Kongkitkul et al., 2008a; Duttine et al., 2008). This model was modified by Hirakawa et al. (2003), Kongkitkul et al. (2004) and Tatsuoka et al. (2004) to apply to polymer geosynthetic reinforcement (Fig. 29b).

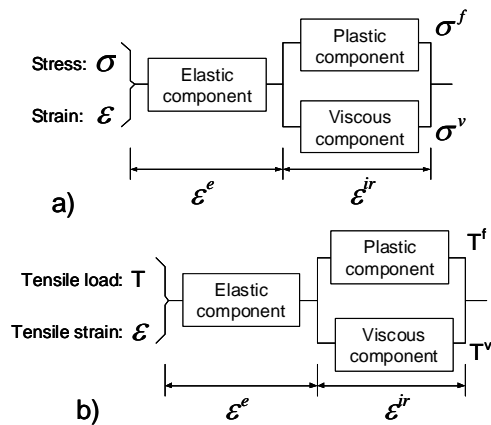


Fig. 29. a) Non-linear three-component model for geomaterials (Di Benedetto et al., 2002; Tatsuoka et al., 2002); and b) non-linear three-component model modified for geosynthetic reinforcement (Hirakawa et al., 2003; Kongkitkul et al., 2004).

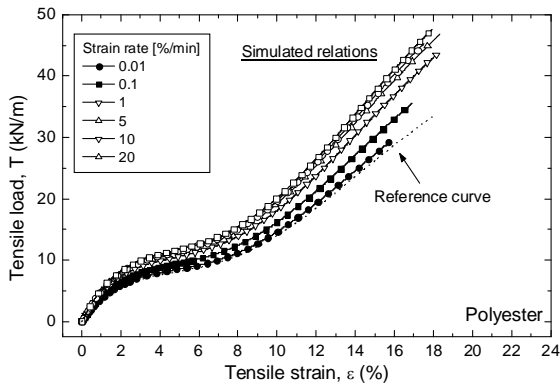


Fig. 30. Simulation of continuous ML tests presented in Fig. 18 by the three-component model (the combined viscosity) PET geogrid (Hirakawa et al., 2004).

According to this model (Fig. 29b), the measured tensile load, T , consists of inviscid and viscous components, T^f and T^v , while the measured strain rate, $\dot{\epsilon}$, consists of elastic and irreversible (or visco-plastic) components, $\dot{\epsilon}^e$ and $\dot{\epsilon}^{ir}$. The elastic component of the model exhibits the hypo-elastic behaviour with a $T - \epsilon^e$ relation having the tangent modulus being a function of T . The plastic (or inviscid) component exhibits the plastic behaviour with a unique rate-independent non-linear $T^f - \epsilon^{ir}$ relation under loading conditions, where the

irreversible strain rate is always positive (i.e., tensile). The viscous component exhibits the viscous behaviour with a highly non-linear rate-independent $T^f - \dot{\epsilon}^{ir}$ relation. With most of polymer geosynthetic reinforcement types, the present tensile load, T , is a unique function of instantaneous $\dot{\epsilon}^{ir}$ and its rate under loading conditions. More details of the model are explained in Hirakawa et al. (2003), Tatsuoka et al. (2004); Kongkitkul & Tatsuoka (2007) and Kongkitkul et al. (2004, 2007a & b).

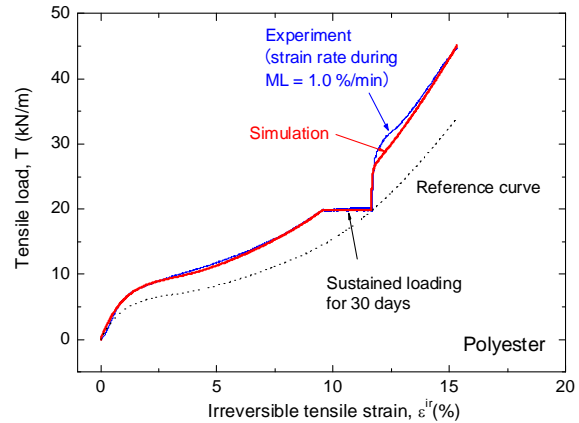


Fig. 31. Simulation of a ML test with 30 day-long SL on a PET geogrid (Fig. 20).

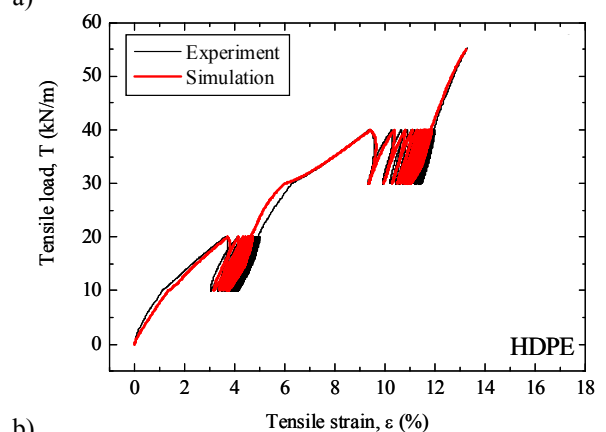
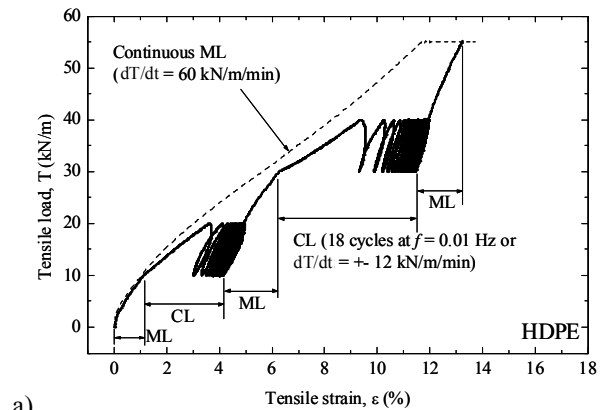


Fig. 32. a) Tensile load-strain relationships from ML tests at a load rate equal to 60 kN/m/min with and without cyclic loading (CL) at $f = 0.01$ Hz with 10 kN/m cyclic amplitude, HDPE geogrid; and b) comparison with simulation (Kongkitkul et al., 2004).

Figs. 30 and 31 show simulations of the tests described in Figs. 18 and 20. It may be seen that the tests are simulated very well by the non-linear three-component model. It may also be seen from **Figs. 32a and b** that cyclic loading tests can also be simulated very well. This simulation shows that residual strains that develop during cyclic loading are due essentially to viscous properties while the inviscid effects of cyclic loading are negligible.

The discussions above indicate that creep is not a degrading phenomenon. Furthermore, Isochronous Concept is unable to properly predict the time-dependent deformation of in-air geosynthetic reinforcement subjected to general arbitrary loading histories: i.e., the use of this quite misleading concept is not beneficial for *Geosynthetic Engineering*.

In-Soil Behaviour of Geosynthetic Reinforcement

Is the tensile force in in-soil reinforcement kept constant ?: In routine design of GRS structures based on the limit-equilibrium stability analysis, only the viscous properties of polymer geosynthetic reinforcement are taken into account in a specific way, while ignoring the viscous properties of the backfill. Moreover, the current design method (Eq. 1) assumes that the tensile force activated in polymer geosynthetic reinforcement is kept constant under long-term fixed static boundary conditions of GRS structure. Then, the possibility of the creep rupture of geosynthetic reinforcement is taken into account by largely reducing the rupture tensile strength obtained by fast tensile loading tests of fresh product using the so-called “creep reduction factor” (Fig. 22). This method is relevant to in-air geosynthetic reinforcement subjected to constant tensile load. However, the reinforcement is an elasto-viscoplastic material and, with GRS structures, it is arranged in the backfill that may exhibit significant rate-dependent (i.e., viscous) behaviour.

Tatsuoka et al. (2004) suggested that the tensile load in polymer geosynthetic reinforcement arranged in typical field full-scale GRS structures subjected to constant load may decrease with time due to the viscous properties of both reinforcement and backfill and interactions between them. Furthermore, they argued that the assumption that constant tensile load is maintained in the reinforcement during the whole design life is usually conservative while over-estimating the possibility of creep rupture of geosynthetic reinforcement. That is, it is unlikely with typical full-scale GRS structures that the tensile rupture of polymer geosynthetic reinforcement becomes imminent during its life time. These arguments have been substantiated by two series of drained plane strain compression (PSC) tests that were subsequently performed on air-dried Toyoura sand specimens unreinforced and reinforced with different types of polymer geogrid that are described below.

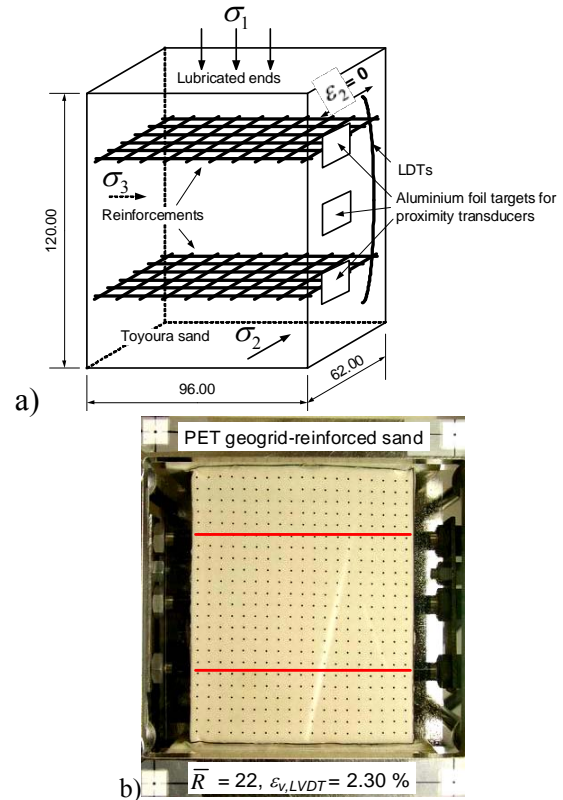


Fig. 33. a) Reinforced Toyoura sand specimen for PSC tests; and b) σ_2 face of a reinforced specimen with markers printed on the membrane (horizontal red lines indicate the locations of geogrid) (Kongkitkul et al., 2007c & d).

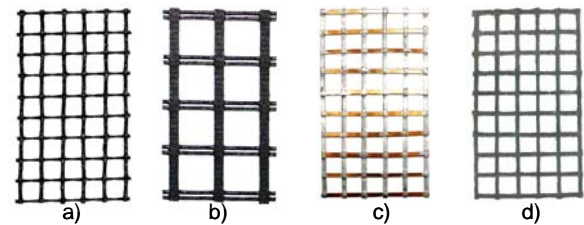


Fig. 34. a) Polyester (PET) geogrid; b) Polyvinyl alcohol (PVA) geogrid; c) smooth phosphor bronze (PB) grid; and d) rough PB grid, used to reinforce PSC sand specimens (Kongkitkul et al., 2007c).

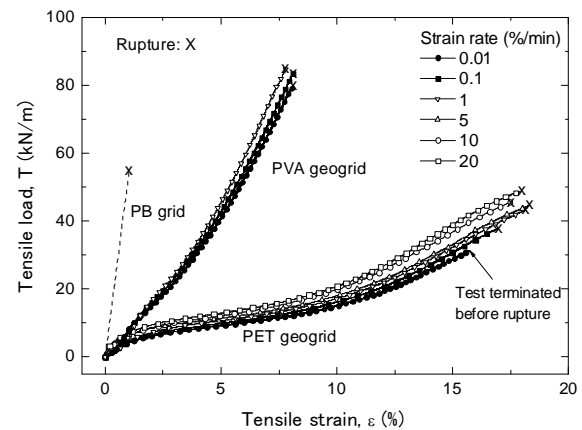


Fig. 35. Tensile load-strain relations of PB grid, PET geogrid and PVA geogrid (Kongkitkul et al., 2007c).

Two series of PSC tests on reinforced sand: The first series (Kongkitkul et al., 2007c & d) used relatively small specimens of dense air-dried Toyoura sand (**Fig. 33**) reinforced with two layers of grids made of polymer geosynthetic reinforcement and phosphor bronze (**Figs. 34 and 35**). Typical PSC test results, obtained by using PET the grid, are presented in **Fig. 36**.

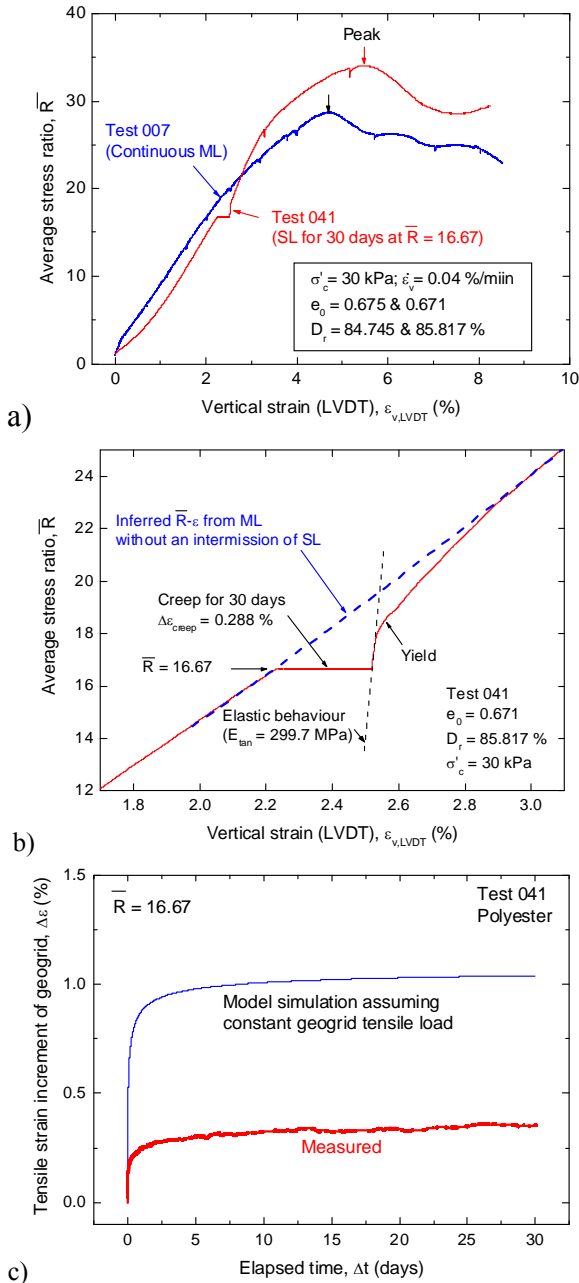


Fig. 36. a) Whole stress-strain relations from PSC tests (0.04 %/min, 30 kPa) on PET reinforced Toyoura sand with a 30 day-long sustained loading stage (test 041) and small unload/reload cycles (test 007); b) zoom-upped relation of test 041; and c) comparison between the time histories of measured average tensile strain in the PET geogrid and strain by simulation assuming a constant tensile load (Kongkitkul et al., 2007d).

As shown in **Figs. 36a and b**, sustained loading (SL) for 30 days was performed during otherwise monotonic loading (ML) at an axial strain rate of 0.04 %/min in test 0041. \bar{R} is the average principal stress ratio defined as $\bar{\sigma}'_v / \sigma'_c$; where $\bar{\sigma}'_v$ is the average vertical stress; and σ'_c is the confining pressure (30 kPa). The axial strain is the value averaged for the whole specimen height. It may be seen from Fig. 36a that the reinforced sand became even stronger by this SL than the one in continuous ML. This trend is due likely to a better interlocking that developed during the SL stage. This result indicates that creep deformation of polymer geosynthetic reinforcement, as well as that of sand, is not a degrading phenomenon for geosynthetic-reinforced soil.

The lower one of the two curves presented in **Fig. 36c** is the time history of measured tensile strain of two geogrid reinforcement layers arranged in sand during SL for 30 days of the reinforced sand specimen described in Figs. 36a and b. The strain was evaluated by the photogrammetric analysis and external measurements of the length of reinforcement (n.b., the details are explained in Kongkitkul et al., 2007d). The upper curve in Fig. 36c is the time history of tensile strain obtained by simulation assuming constant geogrid tensile load based on the non-linear three-component model (Fig. 29b). It can be readily seen that the tensile strain increment of the geogrid placed in sand measured during a 30 day-SL of reinforced sand specimen is substantially smaller than the one estimated assuming that the geogrid tensile load were kept constant. This comparison indicates that, in this test, the tensile load mobilised in the geogrid reinforcement arranged in sand decreased with time during this SL stage of the reinforced sand specimen. Kongkitkul et al. (2007d) reported that the load reduction rate was larger when the stress state during SL was more remote from the failure state of reinforced sand.

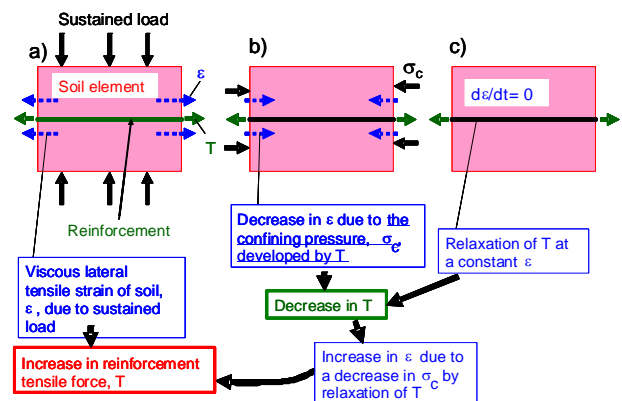


Fig. 37. Interactions between sand and reinforcement (n.b., these figures only schematically describe the average stress and load) (Tatsuoka et al., 2004).

The tensile load and strain state of the polymer reinforcement arranged in a sand specimen subjected to constant sustained load is controlled by the following three factors (**Fig. 37**):

Factor a: An increase with time in the tensile strain in the reinforcement imposed by an increase in the viscous lateral tensile strain of sand that increase with time by sustained vertical loading of the reinforced sand (i.e., viscous Poisson's effects with sand).

Factor b: A decrease with time in the tensile strain in the reinforcement associated with the development of viscous lateral compressive strain of sand that is caused by confining pressure that develops by reinforcement tensile load (i.e., reinforcement-constraint effects).

Factor c: A decrease with time in the tensile load in the reinforcement that would take place even when the tensile strain is kept constant (i.e., the phenomenon of load relaxation).

In the test result presented in Fig. 36, the effects on the tensile strain in the geogrid of factor *a* overwhelm those of factor *b*, therefore, the tensile strain in the geogrid increased with time during the SL stage. On the other hand, the combined effects of factors *b* and *c* on the tensile load in the geogrid overwhelm those of factor *a*, therefore, the tensile load in the geogrid decreased with time during the SL stage.

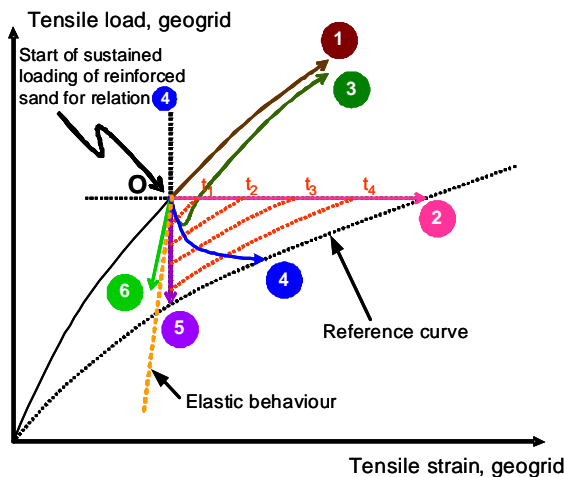


Fig. 38. Schematic diagram of tensile load - tensile strain relations of polymer geosynthetic reinforcement subjected to different loading histories

The considerations above suggest that, depending on loading conditions, as well as structural details, of a given geosynthetic-reinforced soil mass (or structure), the tensile load in the geosynthetic reinforcement may increase, or may be kept constant, or may decrease with time and even unloading may take place. Fig. 38 illustrates schematically the tensile load-strain relations (1 through 6) of geosynthetic reinforcement having elasto-viscoplastic properties when subjected to the following different loading histories starting from a common state, *O*, that has been reached by the same continuous ML at a constant strain rate:

Relation 1: Continuation of ML at the same constant strain rate from state *O* toward the ultimate failure.

Relation 2: SL at a fixed load, as implicitly assumed in the conventional design (Eq. 1 and Fig. 22).

Relation 3: Continuation of ML after a step decrease in the strain rate.

Relation 4: The tensile load decreases with time at a decreasing rate while the tensile strain increases at a decreasing rate.

Relation 5: Relaxation of the tensile load at a fixed strain.

Relation 6: Unloading at negative irreversible strain rates.

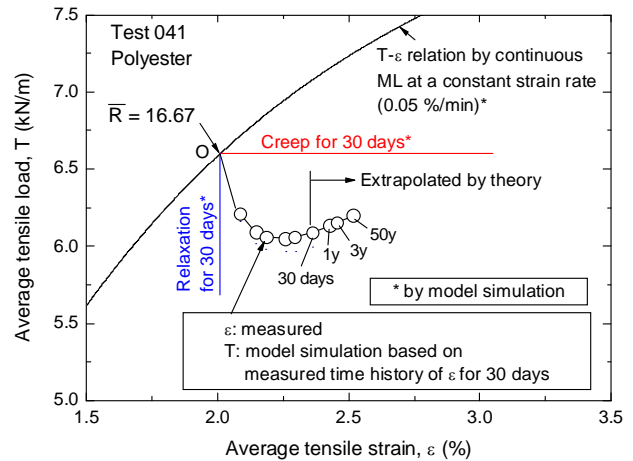


Fig. 39. Tensile load-strain relations of PET geogrid arranged in sand during SL of reinforced sand specimen obtained by the model simulation, compared with relations by SL and load relaxation (Kongkitkul et al., 2007d).

During a 30 day-SL stage of reinforced sand specimen shown in Fig. 36, where the failure of reinforced sand specimen is not imminent, the geogrid reinforcement arranged in sand exhibits relation 4, as shown in Fig. 39 (the details are explained below). In this case, relation 2 largely over-estimates the residual strain in the geogrid (Fig. 36c). In Fig. 38, the contours at the identical elapse times since the start of these different loading histories are presented for stress-strain curves radiating from the same origin with the strain rate decreasing with time, like curves 2, 4 and 5. After an infinite time, all loading paths end at the reference curve (i.e., the load-strain relation without viscous effects, obtained by imaginary ML at zero strain rate).

The tensile load - tensile strain relations of the PET geogrid shown in Fig. 39 were obtained for the following four loading histories by simulations of the test described in Fig. 36 based on the non-linear three-component model:

1. Continuous ML at a strain rate of 0.05 %/min. This strain rate is equal to the one when \bar{R} increased from 13.33 to 16.67 during ML of the reinforced Toyoura sand.
2. SL at a fixed tensile load that lasts for 30 days starting from state *O* where \bar{R} of the reinforced sand specimen is 16.67 and the average tensile strain of the geogrid, $\epsilon_{h,average}$, is 2.01 %.
3. Load relaxation at a fixed strain that lasts for 30 days starting from state *O*.

4. Relation of a geogrid placed in a sand specimen under SL of reinforced sand obtained by simulation based on the three-component model (Fig. 29b) from the measured time history of geogrid strain rate presented in Fig. 36. This behaviour is similar to relation 4 illustrated in Fig. 38.

The relation by loading history 4, presented in Fig. 39, shows that, during the 30 day-long SL of reinforced sand specimen, the tensile load in the PET geogrid first decreases very fast and then becomes rather constant. The geogrid tensile load then starts increasing slightly. However, the increasing rate is very small. According to the model simulation, the geogrid tensile load would be kept significantly lower than the initial value even after an elapsed time of 50 years. Kongkitkul et al. (2007d) reported other similar test results and their simulations.

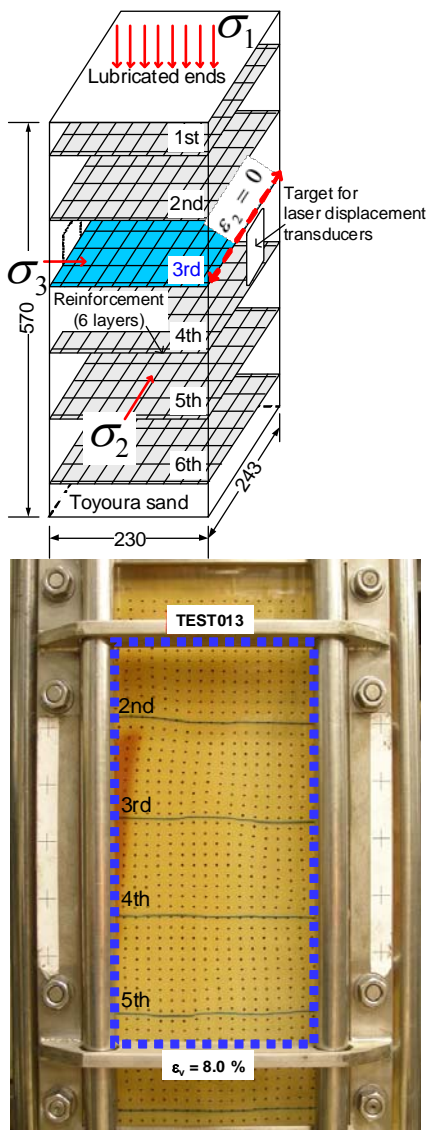


Fig. 40. Large PSC specimen of reinforced Toyoura sand: a) dimensions; and b) σ_2 surface when axial strain = 8.0 %, PET GC-reinforced sand (Kongkitkul et al., 2007e, 2008b).

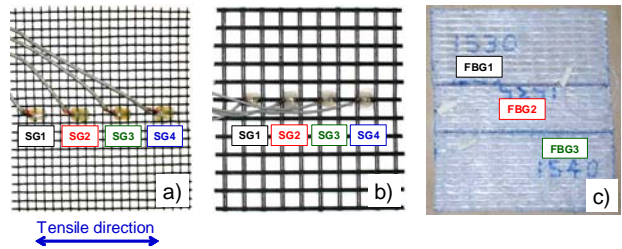
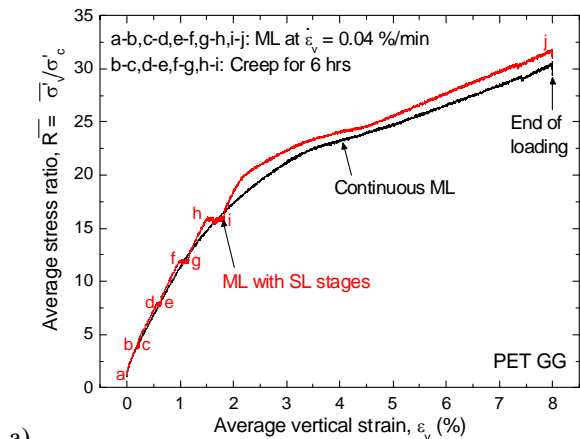


Fig. 41. a) PET GG; and b) PVA GG, both with four electric-resistant strain gauges adhered to a longitudinal member; and c) PET GC with FBG sensors inserted in three longitudinal yarns (Kongkitkul et al., 2008b).

As the specimen size of the first series, described above, is relatively small, to obtain results more representative of field full-scale behaviour, the second series of similar PSC tests were performed on much larger ones (Fig. 40; Kongkitkul et al., 2007e, 2008b). Unlike the first series, local tensile strains of PET GG geogrid and PVA GG geogrid were measured with electric-resistant strain gauges (Fig. 41). The other test conditions are essentially the same as the first series (i.e., air-dried Toyoura sand; the axial strain rate during ML equal to 0.04 %/min; and the confining pressure equal to 30 kPa).

Figs. 42a and b present the $\bar{R} - \varepsilon_v$ relations from two PSC tests on PET GG grid-reinforced sand. The first test is continuous ML. The second test is ML with multiple SL stages. The respective SL stages lasted for six hours. Fig. 42c shows the distributions of measured local tensile strain, ε_{local} (positive in tension), at the start and end of respective SL stages. Fig. 43a shows the time histories of individual local tensile strains and their average. The measured strain values and their average are plotted in the original scale and the scale factored by a ratio of 3.84. This factor was obtained by calibration tests of the geogrid used in the PSC tests. A solid curve presented in Fig. 43b is the time history of factored averaged tensile strain in the PET GG reinforcement before and during SL at $\bar{R} = 12$, obtained from the plot presented in Fig. 43a.



a)

(to continue)

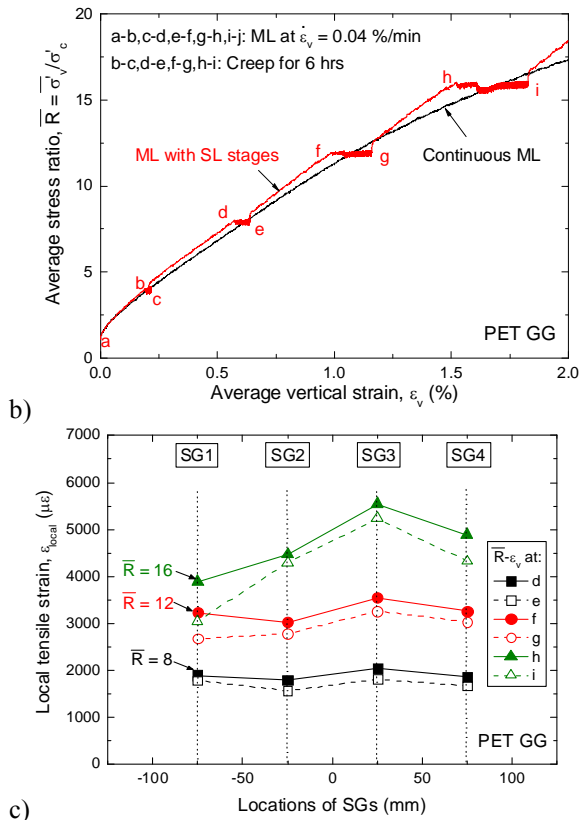


Fig. 42. a) & b) Stress-strain relations of PET GG-reinforced sand subjected to SL during otherwise ML at $\sigma_c = 30$ kPa; and c) distributions of local tensile strain in the PET GG during SL stages (Kongkitkul et al., 2008b).

The following trends of behaviour may be seen from these results:

- 1) Noticeable creep axial strains took place in the reinforced sand at these multiple SL stages, which should be attributed to the viscous properties of both sand and geosynthetic reinforcement while affected by their interactions. The creep axial strain of the reinforced sand increased with an increase in the sustained load.
- 2) When ML was restarted after the respective SL stages, the reinforced sand became slightly stiffer and stronger than the behaviour during continuous ML. This trend is the same as the one seen in Fig. 36a. This result reconfirms that creep deformation is not a degrading phenomenon for geosynthetic-reinforced sand, as for geosynthetic reinforcement. Rather, creep deformation is merely a result of interacting viscous behaviours of sand and geosynthetic reinforcement, which may include some positive ageing effects.
- 3) The local tensile strains measured at all locations of the geogrid noticeably decreased with time at the all SL stages. This trend of behaviour is different from the one that was observed in the first series (Fig. 36).

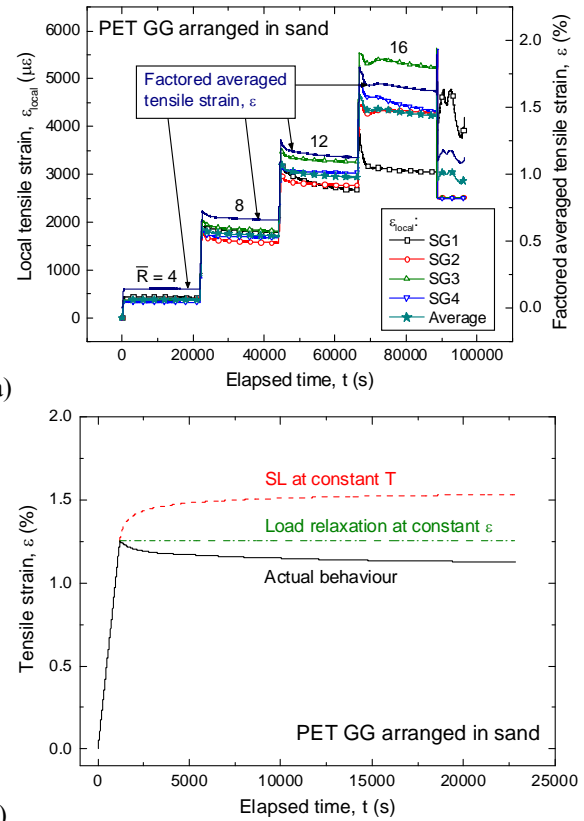


Fig. 43. a) Time histories of individual local tensile strains and their average in the original and factored scales; and b) time histories of factored averaged tensile strain before and during SL at $\bar{R} = 12$, PET GG-reinforced Toyoura sand (Fig. 42) (Kongkitkul et al., 2008b).

In Fig. 43b, the time history of strain obtained by simulation assuming that the tensile load were kept constant at the initial value throughout the SL stage is also presented. The time history if the tensile strain were kept constant is also depicted. **Figs. 44 and 45** show the relationship between the tensile load and strain and the time history of tensile load that was obtained by simulations based on the measured time history of tensile strain of PET geogrid. In Fig. 44, the inviscid load and strain relation (i.e., the reference relation obtained by imaginary ML at zero strain rate) under loading conditions starting from the origin ($T = 0$ & $\epsilon = 0$) as well as the one under unloading condition starting from point A (explained below) are presented. Here, the 'loading' (approaching the tensile rupture condition) and 'unloading' (becoming more remote from the tensile rupture condition) are defined based on the sign of irreversible strain rate, $\dot{\epsilon}^{ir}$. The details are described by Kongkitkul et al. (2008b). The elastic load - strain relation that passes through point A is also presented. In Fig. 45, the time histories of tensile load obtained by simulations performed based on the following three assumptions are also plotted:

- 1) the tensile load is always constant and the same as the initial value (i.e., SL condition);

- 2) the strain rate is always kept zero (i.e., load relaxation condition); and
- 3) the strain rate is always elastic (i.e., purely elastic unloading condition).

Note that the measured strain rate of the geogrid (positive in tension), $\dot{\epsilon}$, during SL of reinforced sand is always negative in the present case. In Fig. 44, until point A since the start of SL, $\dot{\epsilon}$ consists of irreversible and elastic components, $\dot{\epsilon}^{ir}$ and $\dot{\epsilon}^e$, as:

$$\dot{\epsilon} \text{ (negative)} = \dot{\epsilon}^{ir} \text{ (positive)} + \dot{\epsilon}^e \text{ (negative)}. \quad (2)$$

When reaching point A, $\dot{\epsilon}^{ir}$ becomes zero, after which $\dot{\epsilon}^{ir}$ becomes negative: i.e.,

$$\dot{\epsilon} \text{ (negative)} = \dot{\epsilon}^{ir} \text{ (negative)} + \dot{\epsilon}^e \text{ (negative)}. \quad (3)$$

The $T - \epsilon$ curve simulated based on the measured time history of $\dot{\epsilon}$ (negative) is smooth at Point A.

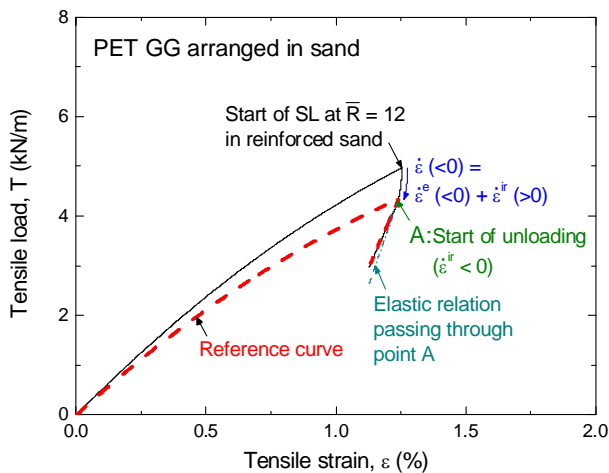


Fig. 44 Simulated relationship between tensile load and tensile strain of PET GG for the time history of tensile strain presented in Fig. 43b (Kongkitkul et al., 2008b).

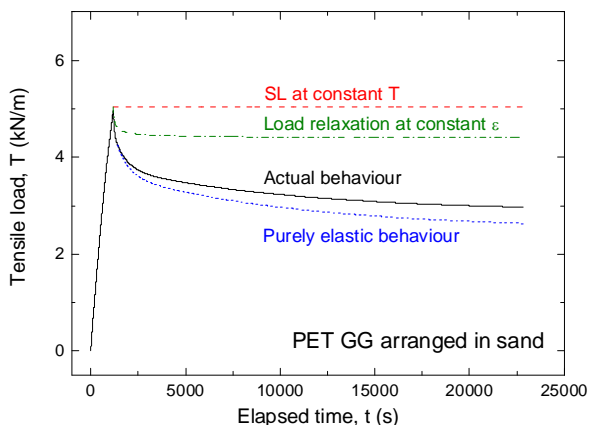


Fig. 45. Time histories of tensile load in the PET GG during SL of reinforced sand at $\bar{R} = 12$, compared with those obtained by simulations for various assumptions (Kongkitkul et al., 2008b).

It may be seen from these figures that the tensile strain in the geosynthetic reinforcement arranged in sand significantly decreased with time during SL of geosynthetic-reinforced sand. This was due to that compressive creep strain in the lateral direction in sand caused by tensile load in the reinforcement (i.e., factor b in Fig. 37) was significant in this case, despite that the global axial strain of the geosynthetic-reinforced sand significantly increased with time (factor a). During this SL stage of geosynthetic-reinforced sand, the tensile load in the geosynthetic reinforcement decreased significantly at a rate higher than the one during the load relaxation stage at a fixed strain. That is, the tensile load-strain state of geosynthetic reinforcement became even under unloading conditions during SL of geosynthetic-reinforced sand. This situation is different from the one observed in the first series PSC test on a small specimen of PET-reinforced sand (Fig. 39).

Summary: Two series of PSC tests on geosynthetic-sand specimens showed that, also with geosynthetic-reinforced soil subjected to vertical compression, creep is not a degrading phenomenon. That is, the compressive strength at the same strain rate of a soil mass reinforced with a polymer geosynthetic does not decrease because of SL histories applied in the pre-peak regime unless time-dependent chemical and/or biological deterioration takes place in the reinforcement. The test results also showed that the tensile load acting in the geosynthetic reinforcement arranged in the backfill under static working load conditions tends to decrease with time by a stress relaxation phenomenon and creep deformation of the backfill. It is likely that the above is also the case with ordinary GRS structures having a sufficient safety factor under static loading conditions. Therefore, it is likely that it is overly conservative to assume in design that the tensile load in the geosynthetic reinforcement arranged in GRS structures subjected to long-term *static working load* is maintained constant as long as the structure are duly designed and constructed. It should be particularly the case when proper seismic-resistant design is made. A case history that shows the above is shown below.

Geosynthetic Reinforcement in Full-Scale Walls

As far as the author knows, there is no case of ordinary permanent geosynthetic-reinforced soil structures that deformed too largely or collapsed due to, respectively, too large creep deformation or creep rupture of geosynthetic reinforcement. A typical case history substantiating the above is “Fujisan-Shizuoka Airport” in Shizuoka Prefecture in Japan, which is now under construction. In this project, two high GRS walls (16.7 m-high and 21.1 m-high) were constructed in two valleys to preserve natural environment consisting of steep swamp areas in front of the walls, which are to be buried in the backfill if gentle-sloped embankments were constructed (Fig. 46).

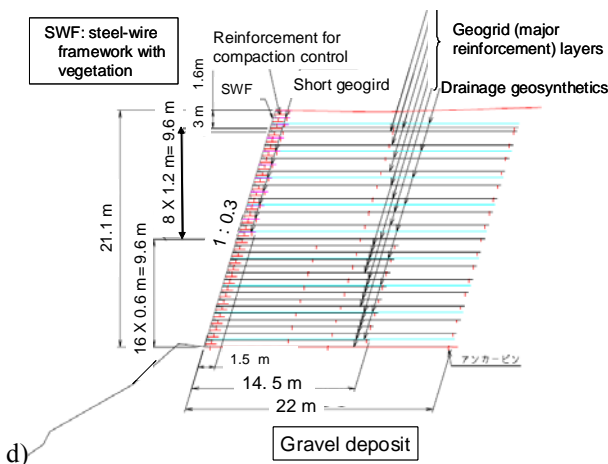
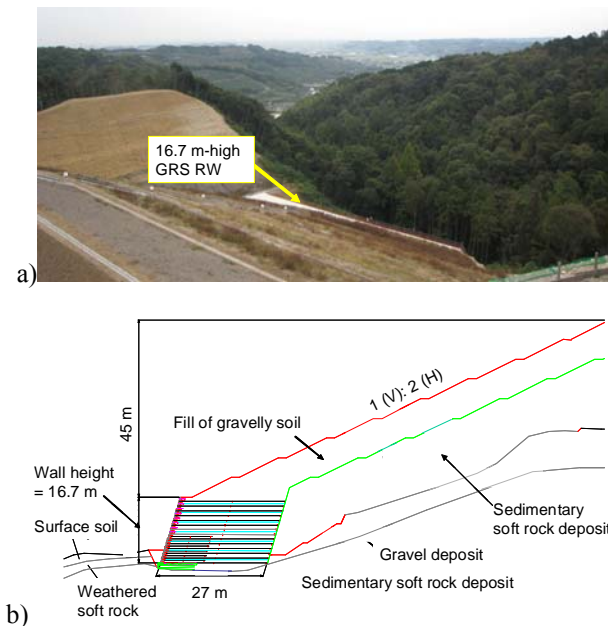


Fig. 46. High GRS walls for Fujisan-Shizuoka Airport; a) back view; and b) cross-section of the wall in valley 1; and c) front view; and d) cross-section of the wall in valley 2 (Fujita et al., 2008).

Figs. 46b and **d** show the cross-sections of the two walls. As the walls support the west side of the runway of the airport, it is required to ensure minimum residual displacements at the crest of the walls. A sufficient high seismic stability is another important design factor. To satisfy these requirements, well-graded gravelly soil (**Fig. 47**) was selected as the backfill, which was compacted

very well to an average degree of compaction higher than 95 % based on the maximum dry density obtained by using compaction energy 4.5 times higher than the standard Proctor (**Fig. 48**).

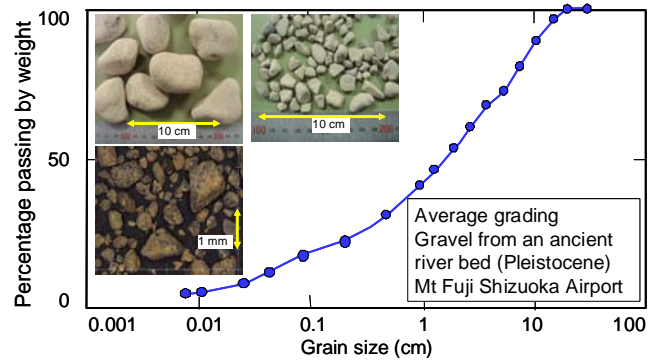


Fig. 47. Average grading curve and particle pictures of the backfill for the wall in valley 2 of Mt. Fuji Shizuoka Airport (Fujita et al., 2007; Takagi et al., 2007)

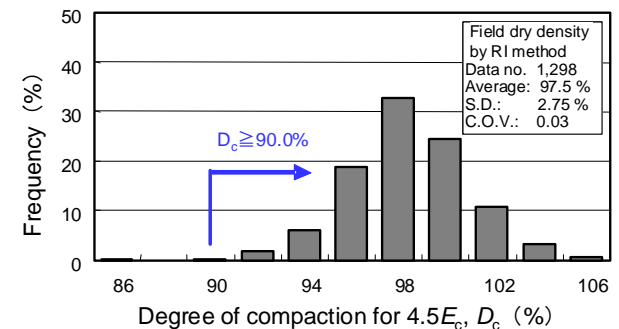
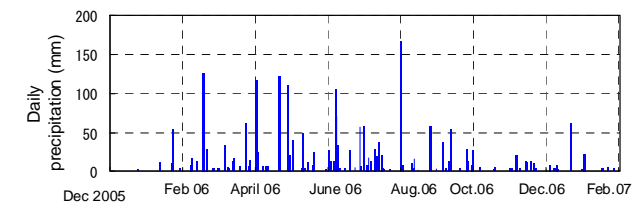
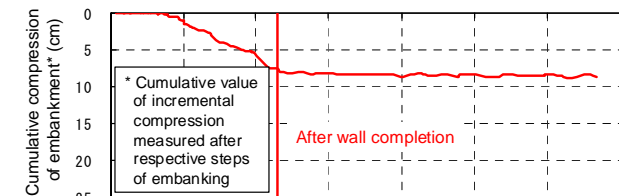
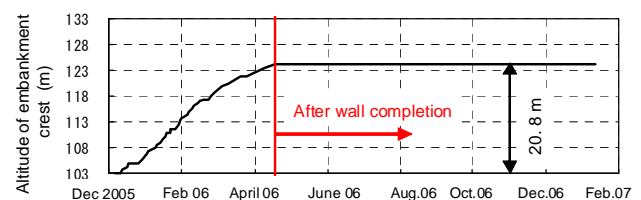
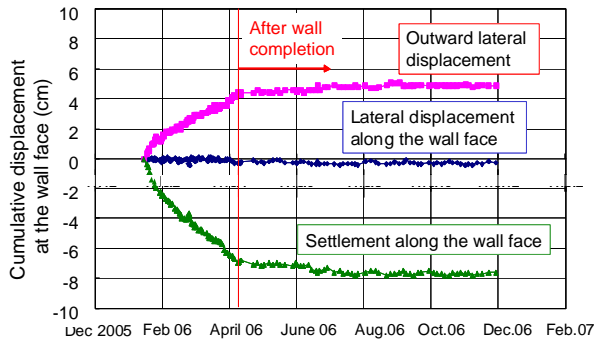


Fig. 48. Distribution of measured D_c of backfill in the wall in valley 2 at Mt. Fuji Shizuoka Airport (Fujinami et al., 2007 & 2008; Fujita et al., 2007a&b; Takagi et al., 2007).



a) (to continue)



b)
 Fig. 49. a) Settlement at the crest of wall (location A in Fig. 50); and b) displacements at wall face (location B in Fig. 50) during and after construction in the wall in valley 2 (Fujinami et al., 2007; Fujita et al., 200, 2008; Takagi et al., 2007).

The field observations of the walls (**Fig. 49**) showed very small instantaneous deformation of the walls during construction and nearly null post-construction residual deformation (see **Fig. 50** for the locations of measurements). It is to be noted that the total vertical compression of the backfill during construction is as small as only 0.5 % of the final wall height. This result indicates a very high stability of the walls under static loading conditions. This case history indicates that long-term residual deformation of geosynthetic-reinforced soil structures can be restrained very effectively by good compaction of the backfill despite that significantly stiff reinforcement members, such as those made of steel, was not used (this issue is discussed again later).

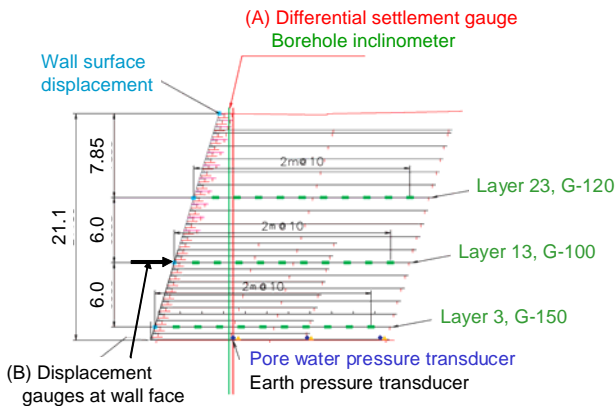


Fig. 50. Locations of geogrid layers equipped with electric-resistant strain gauges, displacement gauges and others in the wall in valley 2; unit in m (Fujinami et al., 2007; Fujita et al., 2007; Takagi et al., 2007; Kongkitkul et al., 2008c).

As typically seen from **Fig. 51**, the recorded time histories of tensile strain in the geogrid also exhibited nearly no increase after wall completion. Kongkitkul et al. (2008c) analysed these data of the wall in valley 2 based on an elasto-viscoplastic constitutive model for polymer geosynthetic reinforcement (Fig. 29b). The

parameters of the model used in this analysis were determined based on the elasto-viscoplastic properties of the geogrid evaluated by a series of tensile loading tests of the geogrid in the laboratory.

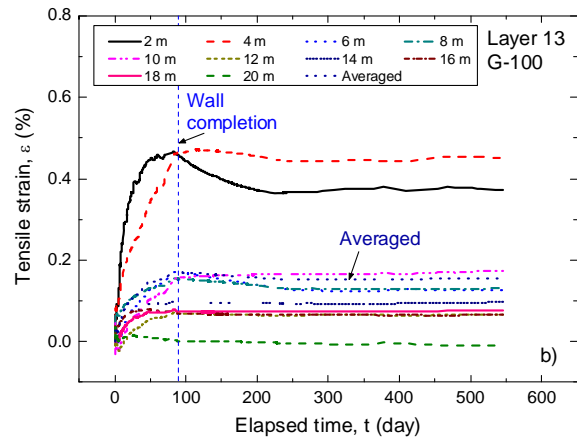


Fig. 51. Time histories of individual and average tensile strains of geogrids arranged in the wall at layer 13 (G-100) in the wall in valley 2 (see Fig. 50 for the location): the legends indicate the distances back from wall face (Kongkitkul et al., 2008c).

Fig. 52 shows the relationships between the estimated tensile load and the measured tensile strain before and after the wall completion in geogrid layers 3, 13 and 23 (Fig. 50) obtained from this analysis. In these simulations, the time histories of average tensile load in the respective geogrid layers arranged in the wall were estimated by the three-component model from the time histories of measured average tensile strain rate until the end of the observation (i.e., 455 days). The strain in the respective geogrid layers is the average of measured values at many different locations (see Figs. 50 & 51). The simulated $T - \epsilon$ relations from the origin (0, 0), which is the moment when the respective geogrid layers were arranged, until the wall completion were obtained from the measured time histories of tensile strain until the wall completion. The dotted curves represent the relations if ML had continued at the strain rate that was observed when the wall was completed. The simulated relations after the wall completion were obtained based on the respective observed time histories of tensile strain rate until the final day of measurement (455 days). The relations were then extrapolated to 50 years by model simulation. When the irreversible strain rate, $\dot{\epsilon}^{ir}$, becomes negative via a neutral state (where $\dot{\epsilon}^{ir} = 0$) from the loading condition (where $\dot{\epsilon}^{ir} > 0$) in the simulation of the post-construction behaviour, the tensile load-strain behaviour enters an unloading branch (where $\dot{\epsilon}^{ir} < 0$).

The trend of behaviour in geosynthetic reinforcement layer 23 after the wall completion (Fig. 52c) is similar to the one presented in Fig. 39, obtained from a PSC test on a small geosynthetic-reinforced sand specimen. That is, the tensile strain rate increases with time, but it is at a

largely decelerating rate. As a result, the $T - \varepsilon$ relations exhibit firstly a fast reduction, which is followed by a gradual increase in the tensile load with time. Even after 50 years, however, the estimated tensile load is only slightly higher than the value at the wall completion. **Fig. 53** shows the time history of tensile load estimated based on the measured tensile strain, corresponding to Fig. 52c. The trends of behaviour described above can be confirmed from this figure. It is also predicted that the tensile load is kept nearly constant after the elapsed time becomes about two years.

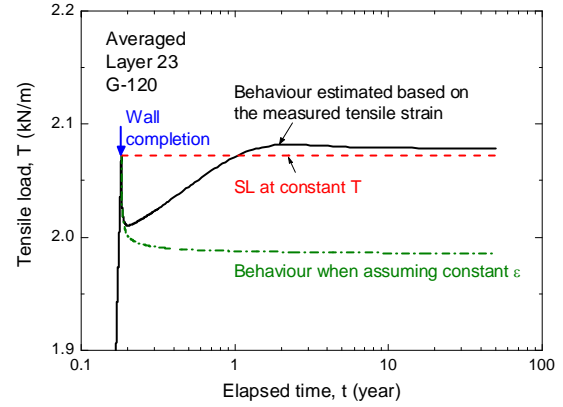


Fig. 53. Estimated time histories of tensile load of geogrid based on averaged strain in layer 23 (Fig. 52c) and the behaviours when assuming constant tensile load and strain (Kongkitkul et al., 2008c).

On the other hand, the trends of behaviour in layers 3 and 13 (Figs. 52a & 52b) are similar to the one presented in Fig. 44, obtained from a PSC test on a large geosynthetic-reinforced sand specimen. That is, the tensile load decreases with time at a high rate due to consistently negative strain rates after wall completion. In these cases, the tensile load decreases firstly under the loading condition (where $\dot{\varepsilon}^{ir} > 0$), then under the unloading condition (where $\dot{\varepsilon}^{ir} < 0$). When estimated assuming purely elastic response under the unloading condition in the simulation, the decrease in the tensile load is largely over-predicted.

Figs. 55 and 56 show typical time histories of strains observed in geogrid layer 13 and results of simulation of the strains observed in three geogrid layers for the wall in valley 1, similar to those for the wall in valley 2. **Fig. 54** shows the locations of these grid layers. In this case, a 45 m-high slope was constructed back of the wall for a period of about nine months starting about two months after the wall completion. Therefore, the geogrid strain tended to increase by load from the slope for some period after the wall completion. Despite the above, the general trends of behaviour seen in Figs. 55 and 56 are similar to those seen in the geogrid layers in the wall in valley 2.

It is shown above that the tensile load in the geogrid tends to decrease with time after wall completion and the creep rupture failure of the geogrid by the end of design life is not likely in this field full-scale case. It should also be the case with GRS structures constructed using well-controlled backfill following construction procedures as in this case. This case history indicates that the assumption in the current practice that the tensile load activated in the geosynthetic reinforcement arranged in the backfill is kept constant over-estimates, perhaps largely, the possibility of creep rupture failure of geosynthetic reinforcement. In the seismic design practice of GRS-RWs having a stage-constructed FHR facing, the rupture strength of geosynthetic-

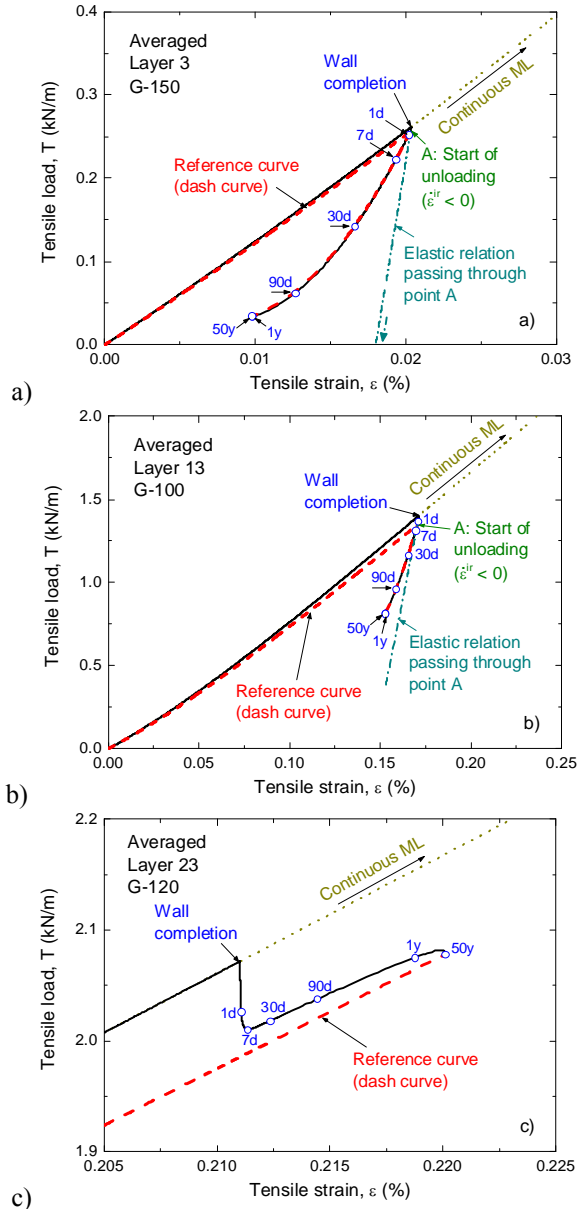


Fig. 52. Tensile load-strain relations of geogrid arranged in the wall in valley 2, averaged for all the locations, predicted for 50-year service, in layers: a) 3 (G-150); b) 13 (G-100); and c) 23 (G-120) (Kongkitkul et al., 2008c).

reinforcement is not reduced for creep rupture. A new method in which the design rupture strength of geosynthetic reinforcement to be used is not reduced for creep rupture for both seismic and static designs of GRS RWs is proposed later.

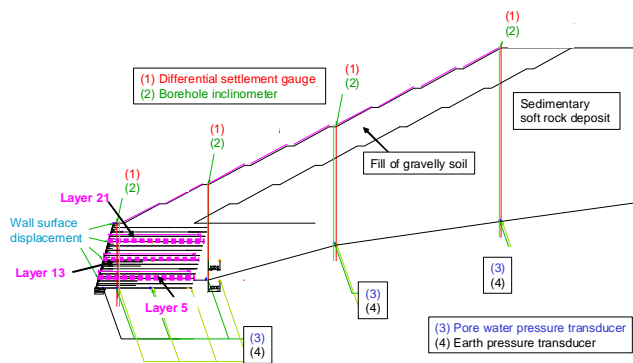


Fig. 54. Locations of geogrid layers equipped with electric-resistant strain gauges, displacement gauges and others in the wall in valley 1 (Fujinami et al., 2007; Fujita et al., 2007; Takagi et al., 2007; Kongkitkul et al., 2008c)

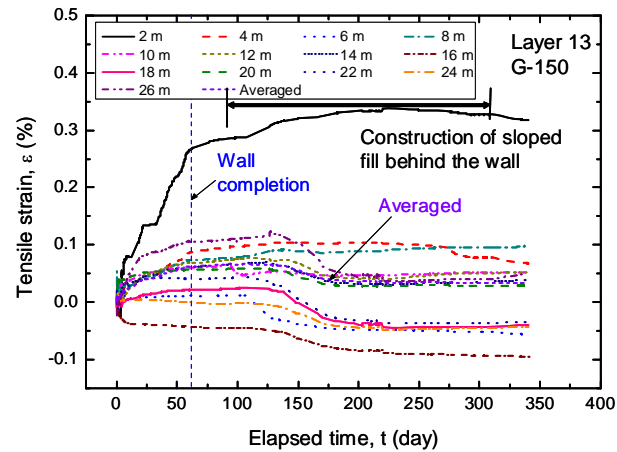


Fig. 55. Time histories of individual and average tensile strains of geogrids arranged at layer No.13 (G-100) in the wall in valley 1: the legends indicate the distances back from wall face (Kongkitkul, 2008d).

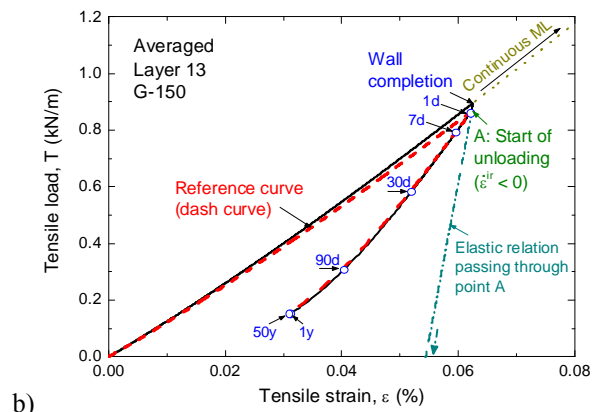
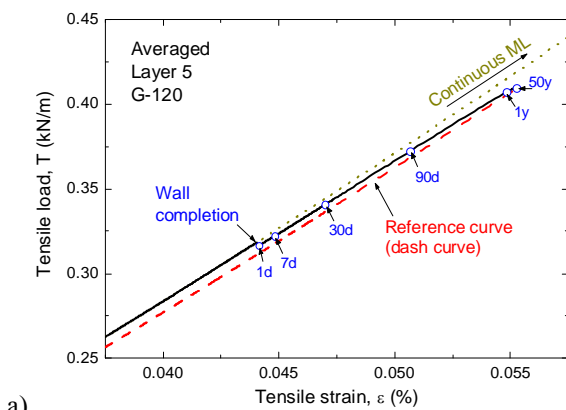


Fig. 56. Tensile load-strain relations of geogrid arranged in the wall in valley 1, averaged for all the locations, predicted for 50-year service, in layers: a) 3 (G-150); b) 13 (G-100); and c) 23 (G-120) (Kongkitkul, 2008d)

Behaviour of Polymer Geosynthetic-Reinforced Soil

It is shown above that it is quite possible to design and construct reinforced soil walls that exhibit very small residual deformation by using so-called extensive reinforcement (i.e., polymer geosynthetic reinforcement). The first reason for the above is that, as the typical backfill has no or nearly zero tensile strength, despite that it is generally much softer than metal reinforcement, geosynthetic reinforcement can reinforce the backfill effectively if the reinforcement layers are adequately arranged and the backfill is well compacted. Secondly, as the typical backfill has significantly viscous properties, even when the backfill is reinforced with metal reinforcement, reinforced soil structures may exhibit significant creep deformation, in particular when reinforcement layers are not adequately arranged or/and the backfill is not well compacted. It is shown below that, drained PSC tests on reinforced sand, the stiffness of reinforced soil may not increase proportionally to an increase in the stiffness of reinforcement.

Effects of reinforcement type: To evaluate the effects of reinforcement stiffness on the strength and deformation of reinforced sand, Kongkitkul et al. (2007c) performed PSC tests on small specimens of dense air-dried Toyoura sand (Fig. 33a) reinforced with

two reinforcement layers of the following different reinforcement types (Fig. 34):

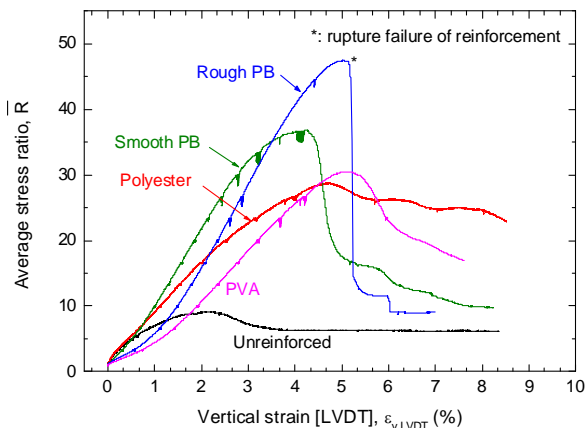


Fig. 57. Average stress ratio and average vertical strain relations from continuous ML PSC on unreinforced and reinforced specimens (average axial strain rate = 0.04 %/min and confining pressure = 30 kPa) (Kongkitkul et al., 2007c).

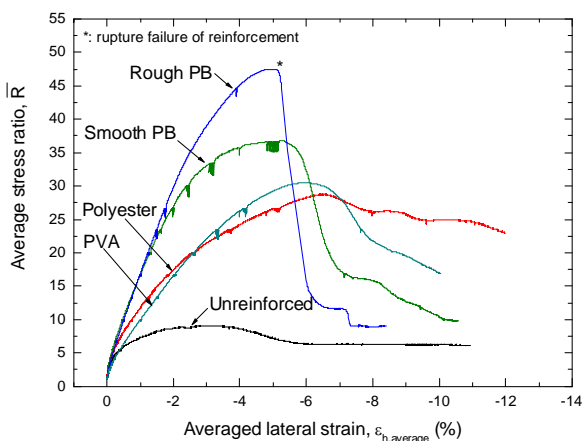


Fig. 58. Average stress ratio and average lateral strain relations corresponding to Fig. 57.

- A polyester (PET) geogrid of biaxial type, consisting of 2 mm-wide x 0.2 mm thick strands with a centre-to-centre spacing of 9 mm. The covering ratio (CR) (i.e., the ratio of the area of reinforcement covering a given plane to the area of the plane) is 22.2 %. A single grid layer consisted of six and ten strands in the longitudinal and transverse directions.
- A Vinylon geogrid of single-axial type, consisting of polyvinyl alcohol (PVA) fibre in both longitudinal and transverse directions with a centre-to-centre spacing between two adjacent members of 20 mm in both longitudinal and transverse directions and CR = 25 %. Each longitudinal member is 5 mm-wide x 1 mm-thick. A single grid layer consisted of three and five strands in the longitudinal and transverse directions.
- A smooth PB grid, consisting of 2 mm-wide phosphor bronze (PB) strips prepared by cutting a 0.2 mm thick PB plate, which were arranged to have the same geometry as the PET geogrid. Each junction, where the

longitudinal and transverse strips were intersected, was fixed using solder.

- A rough PB grid, made by making rough the surface of smooth PB grid by gluing a sheet of non-slip type water-proof corundum C1200 (the JIS standard) sand paper using a rapidly high-strength type glue.

Fig. 35 shows the tensile load - tensile strain relations of these grids.

Fig. 57 shows the average stress ratio – average vertical strain relations from ML PSC tests. Fig. 58 shows the corresponding relationships between average stress ratio – average lateral strain. It may be seen that the pre-peak stiffness when reinforced with rough and smooth PB grids are noticeably higher than those when reinforced with PVA and PET geogrids, which could be attributed to their higher stiffness. Yet, the effects of reinforcement stiffness on the stiffness of reinforced sand are much less significant than the difference in the reinforcement stiffness (Fig. 35). This is because the deformation of the reinforced sand specimen is controlled largely by the deformation of sand. It is therefore likely that it is also the case with field full-scale reinforced structures. Moreover, Kongkitkul et al. (2007e) shows that the effects of micro-structures of geosynthetic reinforcement could be more important than the stiffness of reinforcement.

Furthermore, high compaction and good drainage of the backfill could be equally, or sometime more important than the use of stiff reinforcement. As demonstrated by the case study of Shizuoka walls (Figs. 46 through 56), long-term residual deformation of reinforced soil structures can be restrained very effectively by better compacting the backfill (i.e., by a smaller lift with a higher compaction energy at a relevant water content) using better soil type (i.e., more drainable and easily compactable), without using so-called inextensible reinforcement. In addition, proper arrangements of drainage system designed so that high positive excess pore water pressure does not build up inside the reinforced backfill zone and in the adjacent zones is essential to keep the residual deformation of reinforced soil structures in many wet countries. Shibuya et al. (2007) reported a case history in which a large-scale reinforced soil retaining walls with the backfill reinforced with so-called inextensible reinforcement (i.e., metal strip reinforcement) fully collapsed by heavy rainfall. The major cause for this failure is that, despite that the wall was constructed in a water-collecting valley, no relevant drainage system was arranged inside the wall. Another retaining wall with the sand backfill reinforced with metal strip reinforcement, having no relevant drainage system, was seriously damaged during the 2004 Niigata-ken Chuetsu Earthquake (Kitamura et al., 2005; JGS, 2007). These case histories show that the principles of *Geotechnical Engineering* are often ignored in practice of reinforced soil RWs.

Based on the results from laboratory tests and the field full-scale case histories described above, we can see that it is not relevant to remark that polymer geosynthetic reinforcement is generally inferior to metal reinforcement in constructing reinforced soil structures (i.e., steep-sloped embankments and soil retaining walls) allowing a limited amount of deformation.

SOME DESIGN ISSUES

Design Shear Strength and Stability Analysis of the Backfill

Design versus reality: The actual stress-strain behaviour of soil is very complicated, as schematically illustrated in Fig. 59a. In ordinary *Geotechnical Engineering* practice, however, the design shear strength of backfill is usually determined assuming perfectly-plastic properties (Fig. 59b). Moreover, standard shear strength parameters for respective categorized soil types are often used; e.g., angles of internal frictions (with $c=0$), ϕ_0 , equal to 35° for sandy soil and 40° for gravelly soil are typical values. These standard design shear strengths are similar to, or slightly smaller than, the residual strengths and, therefore, their use could be considerably conservative with ordinarily compacted backfill of GRS RW, as typically shown below.

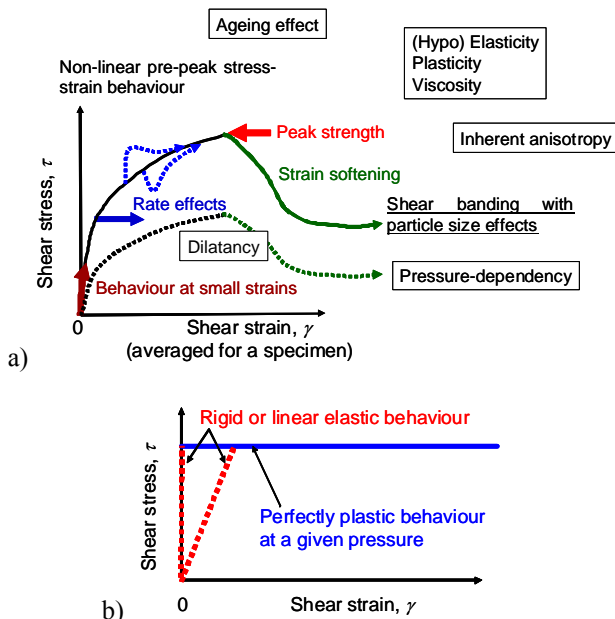


Fig. 59. Schematic diagrams illustrating: a) complicated and difficult stress-strain behaviour of geomaterial; and b) simplified stress-strain models usually employed in routine design practice.

Fig. 60 shows compaction curves of two typical types of backfill obtained by using two levels of compaction energy. Inagi sand ($D_{max}=2$ mm; $D_{50}=0.16$ mm; & $FC=19$ %, Fig. 61) is a sandy soil from a Pleistocene sand deposit currently located above the ground water table in the field. This type of sand is often used as the backfill

for embankments for highways and residential areas in the Tokyo Metropolitan Area. Fig. 62 shows results from drained PSC tests on this Inagi sand. The specimens were 8 cm-wide in the σ_3 direction, 16 cm-long and 20 cm-high. In these PSC tests, the specimens were compacted at the optimum water content (Fig. 60a) and sheared under fully saturated conditions.

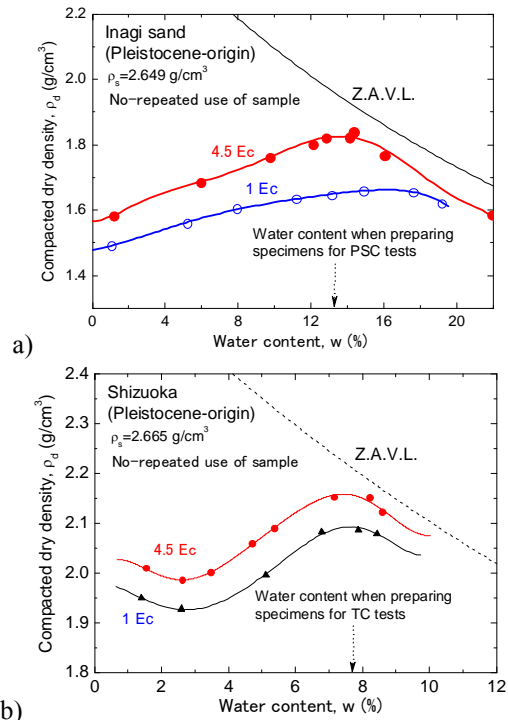


Fig. 60. Compaction curves for two different compaction energy levels: a) Inagi sand (Seida et al., 2008); and b) Shizuoka gravel (Tobisu et al., 2008; Hara et al., 2008).

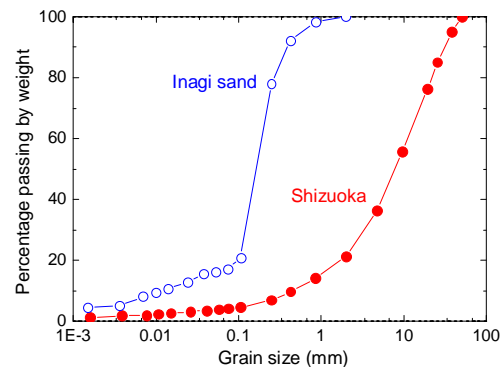


Fig. 61. Grading curves Inagi sand (Seida et al., 2008); and Shizuoka gravel (Tobisu et al., 2008; Hara et al., 2008).

Shizuoka gravel ($D_{max}=50.8$ mm; $D_{50}=8.12$ mm; & $U_c=25.6$ %, Fig. 61) is a well graded round gravelly soil retrieved from a Pleistocene river bed, currently located above the ground water level. The material used in compaction tests and drained TC tests was obtained by removing particles larger than 50.8 mm in diameter from the backfill used to construct high GRS walls for Mt. Fuji Shizuoka Airport (Fig. 47). Fig. 63 shows results

from drained TC tests of large specimens (30 cm in diameter & 58 cm high) of Shizuoka gravel. In these TC tests, the specimens were compacted at the optimum water content (Fig. 60b) and sheared under moist conditions as compacted.

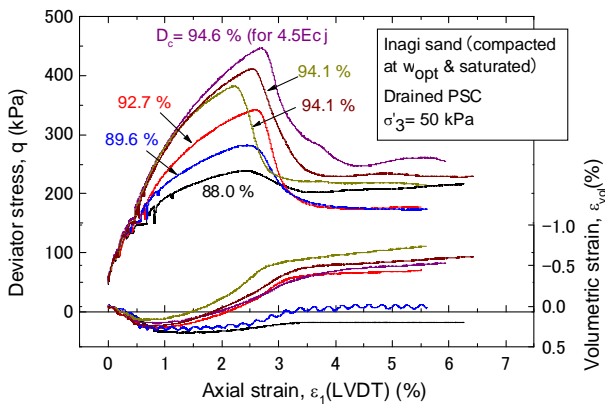


Fig. 62. Results from drained PSC tests on saturated specimens of Inagi sand (Seida et al., 2007, 2008)

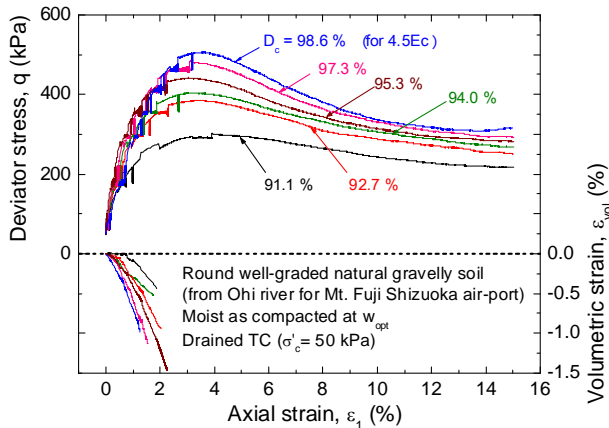


Fig. 63. Results from drained TC tests of moist specimens of well-graded round gravel for Mt. Fuji Shizuoka Airport (Tobisu et al., 2008; Hara et al., 2008).

In the PSC and TC tests described above, the viscous properties of the test materials were evaluated by stepwise changing the axial strain rate and performing SL tests during otherwise ML at a constant strain rate. Although the pre-peak stress-strain curves are affected by this testing procedure, nearly no effects on the peak strength may be seen. It may be seen from Figs. 62 and 63 that, when well compacted, the peak shear strength of sand and gravel is much larger than the respective residual strengths and, therefore, the use of so-called standard design shear strength, which is close to, or noticeably smaller than the residual strength, usually overly under-estimates the true shear strength of well-compacted backfill. This general geotechnical design issue is particularly important when evaluating the stability of soil structures reinforced with planar geosynthetic reinforcement layers with a relatively small vertical spacing (e.g., 30 cm). This is because the backfill can be well compacted by being reinforced with

planar geosynthetic layers with this small vertical spacing, therefore a small compaction lift. In this case, applied compaction energy can be transmitted to the whole height of current compaction lift and lateral yielding of the backfill upon vertical compaction is effectively restrained,

The potential large conservatism in the design shear strength of the backfill discussed above is usually ignored in the design of GRS-RWs. This is another major reason, in addition to large underestimation of geosynthetic strength, why tensile strains measured in the geosynthetic reinforcement arranged in GRS walls are generally much lower than those predicted at the stage of design.

In some countries, the use of residual strength in the design of soil structures, including GRS structures, is positively recommended. However, as the residual shear strength is rather independent of compacted dry density and rather insensitive to soil type, in the design using the residual strengths, it is difficult to take into account the effects of these factors. On the other hand, the peak shear strength of backfill increases with an increase in the compacted dry density, in particular with well-graded coarse materials, and sensitive to soil type. The design shear strengths of backfill used in current design practice in many countries are similar to residual shear strengths, although this similarity is not identified. This situation reflects the current practice of backfill compaction control, as discussed below. Note that the use of peak strength in the stability analysis assuming isotropic perfectly-plastic properties of soil is on the unsafe side. Therefore, stability analysis methods using both peak and residual shear strengths (if possible, also accounting for strain-softening rate and associated progressive failure) becomes necessary, as discussed later.

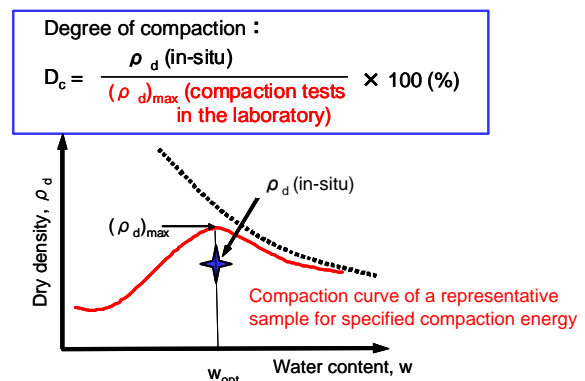


Fig. 64. Definition of the degree of compaction.

Current practice of field backfill compaction control: The current practice is usually based on the degree of compaction (or relative compaction), D_c , defined as the ratio of in-situ dry density to the maximum dry density obtained by compaction tests on a representative sample using specified compaction energy performed in the laboratory (Fig. 64). It is ensured that all values of D_c calculated using the dry densities measured at many

places at a given site be larger than, or equal to, a specified allowable lower limit of D_c . The specified allowable lower limit and the corresponding compaction energy level are different among different countries and different soil structure types. A typical allowable lower limit of D_c is 95 % of the maximum dry density obtained by using compaction energy equal to E_c (i.e., the standard Proctor compaction) or 90 % obtained by using compaction energy equal to $4.5 E_c$. With Inagi sand, $D_c=100\%$ for E_c is equivalent to around 90 % for $4.5E_c$ (Fig. 60a). With Shizuoka gravel, $D_c=95\%$ for E_c is around 92 % for $4.5E_c$ (Fig. 60b). It is shown below that the compaction state when D_c is equal to, or close to, its allowable lower limit is not dense, corresponding to relative low shear strength.

Benefits from better compaction of backfill:

Insufficient compaction of the backfill may result in excessive long-term residual deformation of soil structures, including GRS walls, and serious damage or collapse by seismic loading or heavy rainfall. Therefore, a higher life cycle cost may result from a lower cost used for backfill compaction. On the other hand, as the backfill becomes stronger and stiffer with an increase in the compacted dry density, as typically seen from Figs. 62a and b, a lower life cycle cost becomes possible by better compaction of better backfill type despite higher initial cost at the construction stage.

Fig. 65 summarises the relationships between the peak friction angle, ϕ_0 , and D_c for $4.5E_c$ from many series of drained TC and PSC tests performed at typical operated confining pressures in the field. The following trends of behaviour may be seen from Fig. 65:

- 1) The ϕ_0 value increases at a high rate as D_c for $4.5E_c$ increases from 90 % towards 100 %.
- 2) The ϕ_0 value when $D_c=90\%$ for $4.5E_c$ is noticeably higher than the respective residual strengths, but considerably lower than the peak strengths when D_c for $4.5E_c=100\%$.
- 3) Widely used standard design values of ϕ_0 are lower than the respective values when D_c for $4.5E_c=90\%$.

These trends are usually not taken into account in the current design practice of GRS-RWs, as well as those of ordinary unreinforced embankments. It is likely that this situation reflects the fact that it is generally prohibitively time-consuming, therefore highly costly to perform laboratory stress-strain tests to obtain such a relation as shown in Fig. 65 for a given backfill type for a given construction project. It seems that, as a result, many geotechnical engineers are not well aware of the paramount benefits from better compaction of backfill and they naturally tend to use standard design shear strengths. In important projects, laboratory stress-strain tests of backfill may be performed. Even in this case, the design shear strength may be determined by conservatively assuming that the representative D_c value in the field is equal to its allowable lower limit, say 90 % for $4.5 E_c$, even 90 % for E_c . This design shear strength largely underestimates the true peak shear strength with well-compacted backfill. Furthermore, the effects of compaction density becomes more significant when saturated backfill is sheared undrained than when sheared drained. So, benefits of better compaction become more significant if the saturated backfill is subjected to seismic loading.

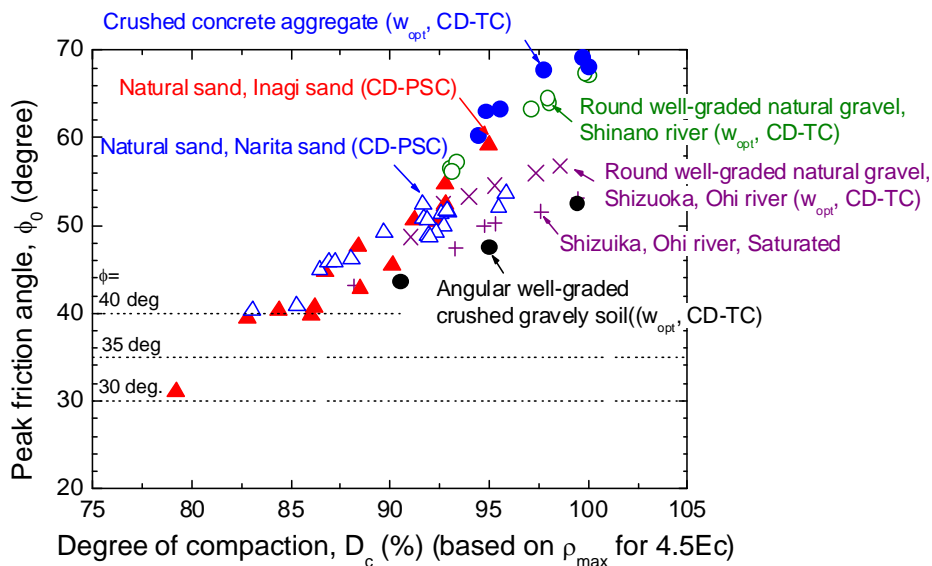


Fig. 65. Summary of $\phi_0 - D_c$ (for $4.5E_c$) relations from drained TC and PSC tests at typical operated confining pressures in the field (mostly around 20 - 50 kPa); the specimens were compacted at w_{opt} (Hirakawa et al., 2008) note: w_{opt} in the parenthesis indicates that the specimens when tested were moist as compacted; the others: the specimens when tested were saturated).

Background for current backfill compaction control:

There is one practical reason for the current practice of backfill compaction control that specifies an allowable lower limits for all measured D_c values (e.g., $D_c \geq 90\%$ for $4.5E_c$ or 95% for E_c) as follows. Fig. 48 shows a typical set of data from backfill compaction control in the field. In this case, the backfill was compacted by using 10 ton-vibratory roller compactors with rather rigorous control of the compacted lift to be equal to 30 cm and the number of roller passing per layer to be equal to eight. Changes in the backfill type from a place to another were relatively small in this project. Despite such modern compaction works as above, the measured D_c values for $4.5E_c$ largely scatter (i.e. S.D. = 2.75 %), between 86 % and 106 %, with an average of 97.5 %. Such a large scatter as above is not an exception, but even larger scatters are often observed in ordinary backfill compaction works. One may consider that such a large scatter in the D_c value as above is due to that compaction efforts by a contractor are not homogeneous at a given construction site. However, this is not the true story. For a nominally the same backfill type, usually a single maximum dry density, $(\rho_d)_{\max}$, is evaluated by a laboratory compaction test using a representative sample of the backfill. Then, the values of ρ_d measured at many places where this nominally same backfill type is used (e.g., for every volume of 1,000 m³ of the compacted backfill in the case of Fig. 48) are divided by this single $(\rho_d)_{\max}$ value to obtain D_c values. Laboratory compaction tests using samples obtained from the respective places where the ρ_d values are measured are usually not performed. Therefore, the true values of $(\rho_d)_{\max}$ at these many places are not known, despite that they must scatter due to inevitable changes in the soil type in terms of grading characteristics and particle properties from a place to another. That is, the D_c values plotted in Fig. 48 are not the true ones, but the apparent ones. The scatter in the true D_c values, if obtained, should be much smaller than the one of the apparent D_c values. As such a large scatter in field measured D_c values (i.e., apparent D_c values) as shown in Fig. 48 is usual, it is evitable to specify the allowable lower limit for all measured D_c values to be equal to the typical lowest value of the apparent D_c values that are usually observed in ordinary backfill compaction works.

In Fig. 48, the average of the measured D_c value is 97.5 %, which is considerably higher than the allowable lower limit (i.e., 90 %). It is very likely that the average of true D_c values (if measured) is similar to that of measured D_c values. In this case, a high average value of measured D_c values, equal to 97.5 %, indicates a very high compaction level of the backfill. This inference is supported by the observations that the total vertical compression during construction of the two embankments (16.7 m and 21.1 m-high) was very small (only about 0.5 %) and essential no residual settlement

has taken place for approximately one year after wall completion (Fig. 49).

The actual practical problem is that the current practice of backfill compaction control specifying an allowable lower limit for all measured D_c values is often misunderstood as follows:

1. The backfill compacted to this allowable limit, or D_c values slightly higher than it, is dense enough.
2. The design shear strength should be (or can be) conservatively determined based on this allowable lower limit of D_c .

Due to the first misunderstanding, it is usual that potential paramount benefits from better compaction are not recognized and not taken into account in design. The second misunderstanding is reflected in low standard design shear strength values. Obviously, the current compaction control and the corresponding use of low standard design shear strength in the current design do not encourage efforts for better compaction using better backfill in field compaction works.

To alleviate these problems, it is firstly necessary that the client of a given project recognizes benefits from better compaction of backfill. The above becomes feasible by using the design shear strength corresponding to the actual compaction state, which is usually significantly higher than the design shear strength currently used in the stability analysis of soil structures when the backfill is well compacted. Then, the contractor should and can receive reward for better compaction of the backfill. In fact, by means of modern mechanical compaction using a reasonable lift (say 30 cm) and a practical number of roller passing, it is not difficult at a reasonable construction cost to achieve actual D_c values that are considerably higher than the allowable lower limit that is usually specified in the current practice of backfill compaction control. The above is usually the case with GRS walls, in particular with GRS-RWs with a staged constructed FHR facing (Fig. 7). This is because the backfill can be compacted well because the lift becomes small corresponding to a small vertical spacing of geosynthetic reinforcement layers and the FHR facing is constructed after the full-height wall has been constructed.

Modified compaction control and modified design shear strength of backfill:

For stricter but more rational field backfill compaction control, it is proposed to specify allowable lower limits not only for all measured values of D_c (e.g., 90 % for $4.5E_c$) but also for their average (e.g., 95 % for $4.5E_c$). This proposal is based on the consideration that the average of measured D_c values be close to the average of true D_c values (if measured). In the case presented in Fig. 48, it is relevant to specify that the allowable lower limit for the average of all measured D_c value for $4.5E_c$ be equal to 95 %.

Having specified the above, it is also proposed to use the peak shear strength corresponding to the allowable

lower limit for the average D_c value in addition to the residual shear strength (or the conventional standard design shear strength) in stability analysis. With the data presented in Fig. 65, the values of ϕ_0 when $D_c=95\%$ for $4.5E_c$ are considerably higher than the respective residual values and the conventional standard design values (e.g., $\phi_0=35^\circ$ for sandy soil and 40° for gravelly soil). Moreover, the dependence of the ϕ_0 value on the soil type increases with D_c . This fact indicates that the importance of taking into account the effects of soil type on the design peak shear strength increases as the backfill is better compacted. If the residual shear strengths or standard shear strengths are used in design, laboratory stress-strain tests are considered useless. On the other hand, when the peak shear strength at a specified well compacted state, as well as the residual shear strength, are used in design, it becomes meaningful to perform proper laboratory stress-strain tests on variously compacted specimens of a given type of backfill.

Stability analysis using peak and residual shear strengths of backfill: To use both peak and residual shear strengths in the limit equilibrium-based stability analysis of GRS RWs that assumes the isotropic perfectly plastic stress-strain properties of the backfill, including seismic stability analysis, it is necessary to properly take into account the effects of inherent anisotropy, the intermediate principal stress (i.e., the b value) and progressive failure on the operational peak shear strength to be used in the stability analysis. In the analysis of active earth pressure and slope stability under essentially plane strain conditions, the peak shear strength evaluated by conventional type drained TC tests can be used by ensuring that the effects of anisotropy and progressive failure are cancelled out by those of the b value.

Fig. 66 shows a stability analysis method using both peak and residual angles of internal friction to evaluate dynamic earth pressure on RWs. This method was developed by modifying the original Mononobe-Okabe seismic earth pressure theory, which assumes isotropic perfectly plastic property of soil. In the particular example described in this figure, the modified theory uses peak and residual friction angles (with $c=0$) as ϕ_0 (peak)= 50° and ϕ_{res} (residual)= 30° . It is conservatively assumed that ϕ_0 drops to ϕ_{res} with zero increment of shear displacement along shear bands. In the conventional seismic design, based on the original Mononobe-Okabe theory with a conservative friction angle, such as 30° , the dynamic earth pressure becomes extremely high when the seismic coefficient becomes higher than a certain value. On the other hand, the use of ϕ_0 (peak)= 50° in the original M-O theory results in too low earth pressures (i.e., on the unsafe side). By the modified M-O theory, we can obtain reasonable values that are between those two unlikely values. Another advantage of the modified M-O theory is that the size of predicted failing active zone is realistically small when

compared with the one obtained by the original M-O theory using the standard design shear strength of the backfill. The modified M-O theory has been adopted in the seismic design codes for railways and highways in Japan (RTRI, 1999 & 2007; JRA, 2002). More details are described in Koseki et al. (2006, 2008).

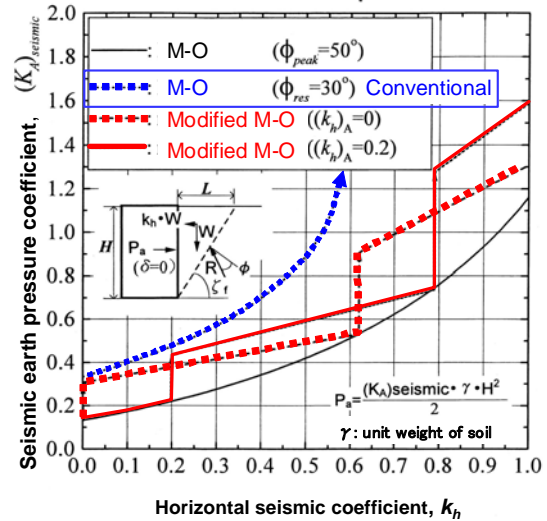


Fig. 66. Modified Mononobe-Okabe dynamic earth pressure theory taking into account peak and residual shear strengths ($c=0$) of the backfill, compared with the original M-O theory assuming isotropic perfectly plastic property of soil (Koseki et al., 1997, 2006, 2008).

Tatsuoka et al. (1998) proposed a limit-equilibrium stability analysis method for GRS RWs having a FHR facing, which is an extension of the modified M-O theory described above. **Figs. 67a** shows a typical wall configuration for which the seismic active earth pressure coefficient $(K_A)_{seismic}$ for the horizontal earth pressure activated along the critical failure planes was evaluated by the following two methods:

- 1) the conventional two-wedge (TW) method that assumes perfectly plastic properties of the backfill using either the peak friction angle ϕ_{peak} ($=45^\circ$) or the residual friction angle ϕ_{res} ($=30^\circ$) with zero cohesion intersect; and
- 2) the modified TW method using both ϕ_{peak} ($=45^\circ$) and ϕ_{res} ($=30^\circ$) with zero cohesion intersect.

The values of the friction angles specified to respective failure planes in these methods are shown in **Fig. 67b**. **Fig. 67c** compares the values of $(K_A)_{seismic}$ when the safety factor for either overturning or sliding failure mode becomes the minimum for all possible combinations of failure planes at respective given horizontal seismic coefficients, k_h . In the modified TW method, it is assumed that the first set of failure planes develop when $k_h=(k_h)_A=0$. This first set of failure planes were sought using the peak friction angle along potential failure planes inside the backfill. At subsequent stages, the friction angle is equal to the residual value. It may be seen from this figure that, similar to the case with unreinforced backfill presented in **Fig. 66**, the modified

TW method yields reasonable earth pressure that is between those obtained by the conventional TW method using ϕ_{peak} and ϕ_{res} .

Fig. 67a compares the critical failure planes evaluated by the conventional and modified TW methods when $k_h=0.5$. The critical failure planes when the backfill is unreinforced obtained by the original M-O method (assuming perfectly plastic properties of the backfill) using either ϕ_{peak} or ϕ_{res} are also presented for reference. **Fig. 67d** compares the size of the failure zone in the backfill, where L^* is the total length of the two wedges on the backfill crest. It may be seen from Figs. 67a and d that the failure zone obtained by the modified TW method is even smaller than the one obtained by the conventional TW method using ϕ_{peak} and substantially smaller than the one obtained by the conventional TW method using ϕ_{res} . In particular, the failure zone evaluated by the modified TW method is much more realistic than the one predicted by the conventional TW method using ϕ_{res} .

In summary, it can be proposed to evaluate the seismic earth pressure acting on along the critical failure plane in the backfill of GRS RW by a modified TW method. This earth pressure should be resisted by reinforcement layers that are extending across the critical failure planes. The modified TW method predicts seismic earth pressure and failure zones that are much smaller than those predicted by the conventional TW method using the conventional design shear strength of the backfill (i.e., the residual shear strength or similar values). When based on the modified TW method, even relatively short reinforcement can increase largely the seismic stability of GRW RWs having a FHR facing, in particular when the seismic load is high. This result is consistent with the field observations and laboratory model tests (Tatsuoka et al., 1998). This feature results from that many reinforcement layers intersect with the potential failure plane (Fig. 67a).

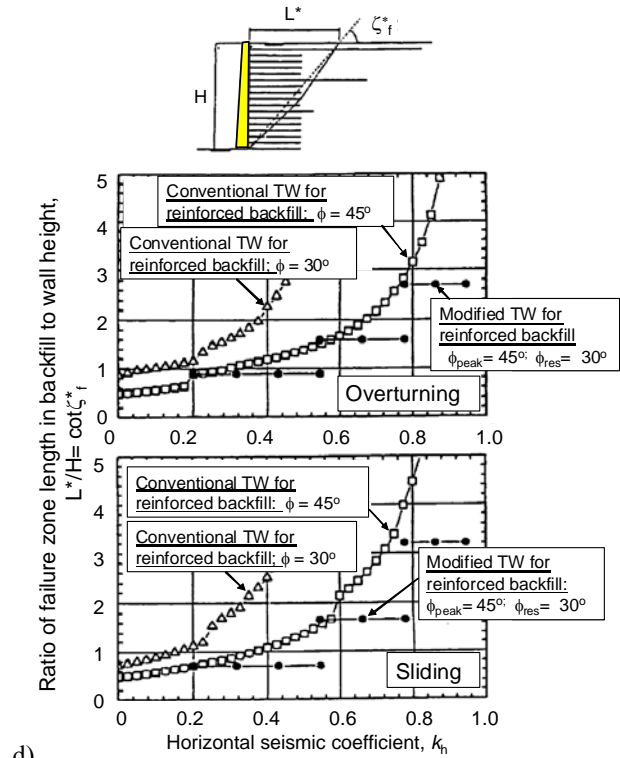
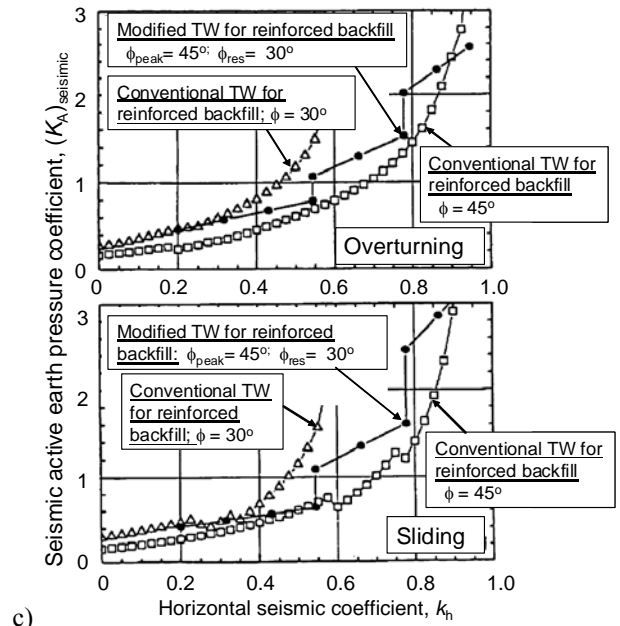
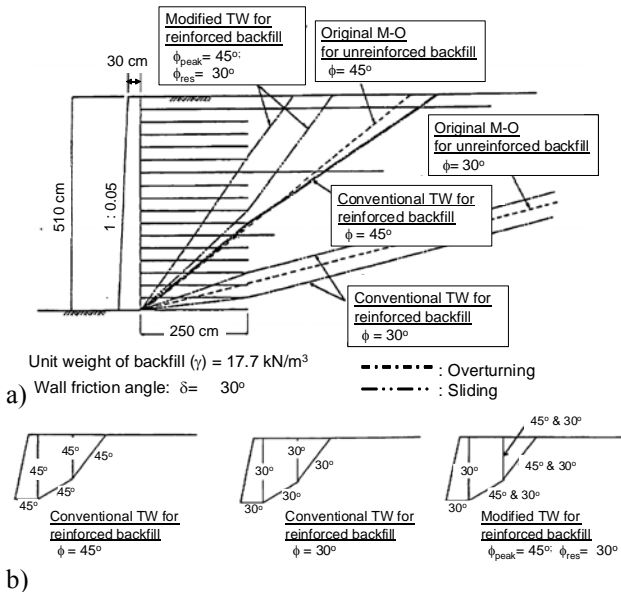


Fig. 67 Comparison between the conventional and modified two-wedge stability analysis for a horizontal seismic coefficient at the initial failure, $(k_h)_A$, equal to 0.2 (Tatsuoka et al., 1998); a) wall configurations with critical failure planes when $k_h=0.5$; b) the values of ϕ used in the analysis (the dimensions are not to scale); c) the seismic earth pressure coefficient (active) acting on the facing $(K_A)_{seismic}$; and d) ratio of failure zone length in the backfill to the wall height.

Leshchinsky (2001) detailed the limit-equilibrium-based stability analysis using both ϕ_{peak} and ϕ_{res} for reinforced soil structures and slopes: i.e., the critical failure plane is

sought by using ϕ_{peak} and the limit equilibriums is evaluated by using ϕ_{res} .

New Design Strength of Geosynthetic Reinforcement

Tatsuoka et al. (2004, 2006) and Kongkitkul et al. (2007b) proposed to introduce the new creep rupture curve (3) shown in Fig. 24 and to obtain the design rupture strength of given geosynthetic reinforcement by Eq. 1 using the creep reduction factor, RF_{CR} , only when necessary. Note that this method becomes more relevant as the backfill is better compacted. The following steps 1 – 5, illustrated in Fig. 68, describe this method:

1. The ultimate tensile rupture strength, T_{ult} , of given geosynthetic reinforcement at a given design strain rate is determined by relevant tensile loading tests using fresh samples. The design strain rate is the value estimated at the moment of failure of a given GRS RW. Design strain rates at failure defined for static and dynamic loading conditions should be different. For example, the strain rate at failure under seismic loading conditions may be higher by a factor of the order of 1,000 than the value under static loading conditions.
2. The value of T_{ult} obtained from step 1 is reduced by a factor of RF_{ID} accounting for installation damage (in the same way as Eq. 1).
3. RF_D to account for chemical and/or biological degradation for the design life is estimated. Then, the value of T_{ult}/RF_{ID} is reduced by a factor of estimated RF_D (in the same way as Eq. 1).
4. It is examined whether the following two conditions are satisfied:

$$(T_d)_{static} \leq \frac{(T_{ult})_{static}}{RF_D \cdot RF_{ID} \cdot (F_s)_{overall,static}} \quad (4a)$$

$$(T_d)_{seismic} \leq \frac{(T_{ult})_{seismic}}{RF_D \cdot RF_{ID} \cdot (F_s)_{overall,seismic}} \quad (4b)$$

where $(T_d)_{static}$ and $(T_d)_{seismic}$ are the design static and seismic working loads that are obtained by relevant stability analysis with $(F_s)_{overall} = 1.0$; and $(T_{ult})_{static}$ and $(T_{ult})_{seismic}$ are the rupture strengths of fresh samples of given geosynthetic reinforcement that can satisfy Eqs. 4a and 4b. It is suggested to use the residual angle of friction as the design shear strength of the backfill for static loading conditions for relevant conservatism at this moment. For seismic loading conditions, it is suggested to use the peak shear strength to locate critical failure planes while the limit equilibrium along the located critical failure planes is evaluated by using the residual shear strength (as the modified TW method described above).

5. Then, the larger value of $(T_d)_{static}$ and $(T_d)_{seismic}$ is chosen. Usually, $(T_d)_{seismic}$ is larger than $(T_d)_{static}$, and

also $(T_{ult})_{seismic}$ that satisfies Eq. 4b is larger than $(T_{ult})_{static}$ that satisfies Eq. 4a. This trend becomes stronger with an increase in the design seismic load.

6. It is confirmed that the design static load, $(T_d)_{static}$, is smaller than the creep rupture strength, $(T_{ult})_{static} / \{RF_{ID} \cdot RF_{CR,m}\}$, that is obtained based on the new creep rupture curve (i.e., curve 3 in Fig. 24). Here, $RF_{CR,m}$ is the modified creep reduction factor which accounts for the effects of simultaneous material degradation and creep deformation. The new creep rupture curve for a given type of polymer geosynthetic reinforcement can be obtained by numerical simulation for given conditions of simultaneous creep rupture and degradation, as described in Kongkitkul et al. (2007b). According to the working examples shown in Tatsuoka et al. (2004), this requirement is usually easily satisfied.

When step 6 is satisfied, the design rupture strength of given geosynthetic reinforcement is determined based on Eq. 1 from which the creep reduction factor, RF_{CR} , is eliminated.

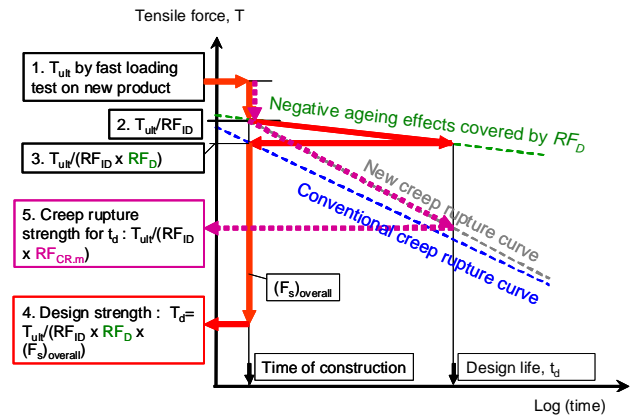


Fig. 68. Newly proposed method to obtain the design strength (not necessarily controlled by creep rupture) of given geosynthetic reinforcement (Tatsuoka et al., 2006; Kongkitkul et al., 2007b).

This newly proposed design method is relevant in particular when a given GRS RW is designed against seismic loads. That is, as $(T_d)_{seismic}$ is usually larger than $(T_d)_{static}$, $(T_{ult})_{seismic}$ usually becomes larger than $(T_{ult})_{static}$. In that case, the creep rupture strength is determined as $(T_{ult})_{seismic} / \{RF_{ID} \cdot RF_{CR,m}\}$. Then, it becomes more likely that the long-term static working load, $(T_d)_{static}$, becomes sufficiently smaller than the creep rupture strength, $(T_{ult})_{seismic} / \{RF_{ID} \cdot RF_{CR,m}\}$.

It is to be noted that the newly proposed method described above is still conservative due to the following two factors:

- 1) It is assumed that the tensile load activated in the geosynthetic reinforcement is kept constant during a given life time.
- 2) Allen and Bathurst (1996) and Greenwood (2002), among others, showed that multiplication of creep

reduction and installation damage factors (Eq. 1) may be conservative.

CONCLUSIONS

From discussions and analyses based on both *Material Engineering for Polymers* and *Geotechnical Engineering* described in this report, we can conclude:

- I. polymer geosynthetic reinforcement is not too extensible and therefore not inferior to metal reinforcement in constructing reinforced soil structures (i.e., steep slopes of embankment and retaining walls) allowing a limited amount of deformation; and
- II. creep rupture failure is usually not an actual major cause for collapse of geosynthetic-reinforced soil (GRS) structures, in particular GRS retaining walls (RWs).

The following more specific conclusions can also be derived:

1. The technology of GRS RW with a stage-constructed full-height rigid facing has become popular in construction permanent important RWs in Japan. In particular, this technology has become the standard RW construction technology for railways in Japan.
2. Creep is not a degrading phenomenon with both geosynthetic reinforcement and backfill, therefore with GRS structures. Creep is merely an elasto-viscoplastic response of material. In the similar way as the shear strength of ordinary type backfill, the tensile rupture strength of geosynthetic is a function of strain rate at rupture irrespective of creep loading history in the pre-peak regime.
3. Corresponding to the above, it is not possible to properly describe and predict the load/stress-strain-time behaviour of backfill and geosynthetic, therefore that of GRS structures, subjected to arbitrary loading histories based on the isochronous concept. On the other hand, the non-linear three-component rheology model described in this paper is relevant to this end.
4. The force that develops in geosynthetic reinforcement that is arranged in field full-scale GRS structures subjected to sustained load may decrease with time unless the safety factor against ultimate failure of structure is very low. In that case, the possibility of creep rupture of geosynthetic reinforcement is usually very low.
5. The design rupture strength of a given type of geosynthetic reinforcement obtained by the current design procedure using a relatively large creep reduction factor determined based on the conventional creep rupture curve could be overly conservative. An alternative new procedure, which is consistent with the ordinary geotechnical design procedure, is proposed.
6. The design shear strength of the backfill of GRS RWs is usually largely under-estimated, in particular when good backfill is well compacted. It is proposed

to modify the current compaction control of backfill by introducing allowable lower limits not only for all measured degrees of compaction but also for their average. It is also proposed to use the peak shear strength corresponding to the allowable lower limit for the average degree of compaction, in addition to the residual shear strength, in stability analysis of GRS-RWs.

ACKNOWLEDGEMENTS

The author sincerely appreciates help in preparing this report of his many current and previous colleagues at the University of Tokyo and Tokyo University of Science, in particular Dr. Kongkitkul, W. (currently Department of Civil Engineering, King Mongkut's University of Technology Thonburi, Thailand) and Dr. Hirakawa, D. (currently Department of Civil and Environmental Engineering, National Defense Academy, Japan), as well as Dr. Tateyama, M. and his colleagues at the Railway Technical Institute, Japan..

REFERENCES

- Aizawa, H., Nojiri, M., Hirakawa, D., Nishikiori, H., Tatsuoka, F., Tateyama, M. and Watanabe, K. (2007). Validation of high seismic stability of a new type integral bridge consisting of geosynthetic-reinforced soil walls, *Proc. of 5th Int. Sym. on Earth Reinforcement* (IS Kyushu), 819-825.
- Allen, T. M. and Bathurst, R. J. (1996). Combined allowable strength reduction factor for geosynthetic creep and installation damage", *Geosynthetics International*, 3(3), 407-439.
- ASTM D4595 *Test Method for Tensile Properties of Geotextiles by the Wide-Width Strip Method*, ASTM International, West Conshohocken, PA.
- Bathurst, R.J. and Cai, Z. (1994). In-isolation cyclic load-extension behavior of two geogrids, *Geosynthetics International*, 1(1), 3-17.
- Bernardi, M. and Paulson, J. (1997). Is creep a degradation phenomenon ?, *Mechanically Stabilized Backfill* (Wu, J.T.H. eds.), Balkema, 329-334.
- Bueno, B. S., Costanzi, M. A. and Zornberg, J. G. (2005). Conventional and accelerated creep tests on nonwoven needle-punched geotextiles, *Geosynthetics International*, 12(6), pp.276-287.
- Bush, D. I. (1986). Variation of long term design strength of geosynthetics in temperature, *Proc. of the 4th International Conference on Geotextiles, Geomembranes and Related Materials*, The Hague, 673-676.
- Christopher, B., Bonczkiewicz, C. and Holtz, R. D. (1994). Design, construction and monitoring of full scale test of reinforced soil walls and slopes, *Recent Case Histories of Permanent Geosynthetic-Reinforced*

- Soil Retaining Walls* (Tatsuoka, F. & Leshchinsky, D. eds.), Balkema, 45-60.
- Di Benedetto, H., Tatsuoka, F. and Ishihara, M. (2002). Time-dependent shear deformation characteristics of sand and their constitutive modelling, *Soils and Foundations*, 42(2), 1-22.
- Di Benedetto, H., Tatsuoka, F., Lo Presti, D., Sauzéat, C. and Geoffroy H. (2005). Time effects on the behaviour of geomaterials, Keynote Lecture, *Proc. 3rd Int. Sym. on Deformation Characteristics of Geomaterials*, IS Lyon '03, Di Benedetto et al. (eds.), Balkema, September, 2003, Vol.2, pp.59-123.
- Duttine, A., Tatsuoka, F., Kongkitkul, W. and Hirakawa, D. (2008). Viscous behaviour of unbound granular materials in direct shear, *Soils and Foundations*, 48(3), to appear.
- FHWA (2001). Mechanically stabilized earth walls and reinforced soil slopes design and construction guidelines, *Federal Highway Administration (FHWA), NHI Course No. 132042*, (Elias, V., Christopher, B.R. and Berg, R.R.), Washington DC, USA, 73, 114-116.
- Fujinami T., Sugimoto T., Nakamura Y., Kawahata S., Funuda H., Yoshida T., Ito M. and Yoshidaaatta N. (2007). Application of reinforced soil wall to high embankment in Mt. Fuji Shizuoka Airport, Part III: Field observation, *Proc. of the 42nd Japan National Conference on Geotechnical Engineering*, Nagoya, paper No.804: 1603-1604 (in Japanese).
- Fujita Y., Sugimoto T., Koha T. and Tsuda M. (2007). Application of reinforced soil wall to high embankment in Mt. Fuji Shizuoka Airport, Part I: Design and planning, *Proc. of the 42nd Japan National Conference on Geotechnical Engineering*, Nagoya, No.802: 1599-1600 (in Japanese).
- Fujita, Y., Sugimoto, T., Nakamura, Y., Kawahata, S., Funada, H., Yoshida, T., Ito, M. and Yoshida, K. (2008). High geogrid-reinforced retaining walls for a new air-port, *Proc. 4th GeoSyntheticsAsia2008*, Shanghai.
- Giroud, J. P. (2008). The Geosynthetics Discipline: Achievements and Challenges, Keynote Lecture, *Proc. the First Pan American Geosynthetics Conference & Exhibition*, 2-5 March 2008, Cancun, Mexico, 1-3.
- Greenwood, J. H. (1994). Designing to residual strength of geosynthetics instead of stress-rupture, *Geosynthetics International*, 4(1), 1-10.
- Greenwood, J. H., Jones, C. J. F. P. and Tatsuoka, F. (2001). Residual strength and its application to design of reinforced soil in seismic areas, *Landmarks in Earth Reinforcement; Proc. of the International Symposium on Earth Reinforcement* (Ochiai et al., eds.), Balkema, 1: 37-42.
- Hara, D., Tobisu, Y., Tatsuoka, F. and Hirakawa, D. (2007). Effects of compaction on drain strength and deformation of saturated gravelly soil, *Proc. 43th National Conference on Geotechnical Engineering, JGS, Hiroshima* (in Japanese).
- Hirai, T. and Yatsu, A. (2000). Evaluation method about tensile strength of geogrid to use for dynamic design", *Journal of Geosynthetics Engineering, IGS Japan Chapter*, 15: 205-214 (in Japanese).
- Hirakawa, D., Kongkitkul, W., Tatsuoka, F. and Uchimura, T. (2003). Time-dependent stress-strain behaviour due to viscous properties of geogrid reinforcement, *Geosynthetics International*, 10(6), 176-199.
- Hirakawa, D., Nojiri, M., Aizawa, H., Nishikiori, H., Tatsuoka, F., Tateyama, M. and Watanabe, K. (2007). Effects of the tensile resistance of reinforcement embedded in the backfill on the seismic stability of GRS integral bridge, *Proc. of 5th Int. Sym. on Earth Reinforcement* (IS Kyushu) (Ochiai et al., eds.), 811-817.
- Hirakawa, D., Kawaharazono, M. and Tatsuoka, F. (2008). Effect of compaction conditions on strength and deformation characteristics of backfill materials, *Journal of Japanese Society for Civil Engineers*, Vol.C-64 (to appear).
- Ishikawa Prefecture (2007). Damage to toll road due to Notohanto earthquake and its rehabilitation, *Official Bulletin*, 1: 4p (in Japanese).
- Japanese Geotechnical Society (2007). Report of Investigation Committee of the Damage by the 2004 Niigata-ken Chuetsu Earthquake (in Japanese).
- Japan Road Association (2002). Specifications for highway bridges, part V - seismic design: pp.65-68. (in Japanese).
- Kazimierowicz-Frankowska, K. (2005). Correlation between the results of creep and relaxation tests of geotextiles", *Geosynthetics International*, 12(5), 269-275.
- Kitamura, Y., Nagao, K., Matsuzawa, K. and Nagakura, H. (2005). Primary field investigation on a Terre Armée Wall subjected to strong seismic load - evaluation of the internal condition and damage state -, *Proc. The 41st Japan National Conf. on Geotechnical Engineering*, Hakodate, Paper No. 981, 1959-1960 (in Japanese).
- Kongkitkul, W., Hirakawa, D., Tatsuoka, F. and Uchimura, T. (2004). Viscous deformation of geosynthetic reinforcement under cyclic loading conditions and its model simulation, *Geosynthetics International*, 11(2), 73-99.
- Kongkitkul, W. and Tatsuoka, F. (2007). A theoretical framework to analyse the behaviour of polymer geosynthetic reinforcement in temperature-accelerated creep tests, *Geosynthetics International*, 14(1), 23-38.
- Kongkitkul, W., Hirakawa, D. and Tatsuoka, F. (2007a). Viscous behaviour of geogrids; experiment and simulation, *Soils and Foundations*, 47(2), 265-283.
- Kongkitkul, W., Tatsuoka, F. and Hirakawa, D. (2007b). Creep rupture curve for simultaneous creep deformation and degradation of geosynthetic reinforcement, *Geosynthetics International*, 14(4), 189-200.
- Kongkitkul, W., Tatsuoka, F. and Hirakawa, D. (2007c). Effects of reinforcement type and loading history on the deformation of reinforced sand in plane strain compression, *Soils and Foundations*, 47(2), 395-414.
- Kongkitkul, W., Tatsuoka, F. and Hirakawa, D. (2007d).

- Rate-dependent load-strain behaviour of geogrid arranged in sand under plane strain compression", *Soils and Foundations*, 47(3), 475-493.
- Kongkitkul, W., Hirakawa, D., Tatsuoka, F., and Kanemaru, T. (2007e). Effects of geosynthetic reinforcement type on the strength and stiffness of reinforced sand in plane strain compression, *Soils and Foundations*, 47(6), 1109-1122.
- Kongkitkul, W. (2008). Analysis of the wall in valley 1 for Fujisan-Shizuoka airport, *Personal communication*.
- Kongkitkul, W., Tatsuoka, F., Duttine, A., Kawabe, S., Enomoto, T. and Di Benedetto, H. (2008a). Modelling and simulation of rate-dependent stress-strain behaviour of granular materials", *Soils and Foundations*, 48(2), 175-194.
- Kongkitkul, W., Hirakawa, D. and Tatsuoka, F. (2008b). Residual deformation of geosynthetic-reinforced sand in plane strain compression affected by viscous properties of geosynthetic reinforcement, *Soils and Foundations*, 48(3), to appear.
- Kongkitkul, W., Hirakawa, D., Sugimoto, T., Kawahata, S., Yoshida, T., Ito, S. and Tatsuoka, F. (2008c). Post-construction time history of tensile force in the geogrid arranged in a full-scale high wall, *Proc. 4th GeoSyntheticsAsia*, Shanghai.
- Koseki, J., Tatsuoka, F., Munaf, Y., Tateyama, M. and Kojima, K. (1997). A modified procedure to evaluate active earth pressure at high seismic loads, *Soils and Foundations, Special Issue*, 209-216.
- Koseki, J., Bathurst, R. J., Guler, E., Kuwano, J. and Maugeri, M. (2006). Seismic stability of reinforced soil walls, Keynote lecture, *Proc. 8th International Geosynthetics Conference (8ICG)*, Yokohama, 51-77.
- Koseki, J., Tateyama, M., Watanabe, K. and Nakajima, S. (2008). Stability of earth structures against high seismic loads, Keynote lecture, *Proc. 13th Asian Regional Conference on Soil Mechanics and Geotechnical Engineering*, 2: (to appear).
- Lee, K., Jones, C. J. F. P., Sullivan, W. R. and Trollinger, W. (1994). Failure and deformation of four reinforced soil walls in eastern Tennessee, *Géotechnique*, 44(3), 397-426.
- Leshchinsky, D., Dechasakulsom, M., Kaliakin, V.N. and Ling, H.-I. (1997). Creep and stress relaxation of geogrids, *Geosynthetics International*, 4(5), 463-479.
- Leshchinsky, D. (2001). Design dilemma: Use of peak to residual strength of soil, *Geotextiles and Geomembranes*, 19(2), 111-125.
- Liu, H. and Ling, H.-I. (2006). Modeling cyclic behavior of geosynthetics using mathematical functions: Masing rule and bounding surface plasticity, *Geosynthetics International*, 13(6), 234-245.
- Maruyama, N., Murayama, M., and Sasaki, F. (2006). Construction of a geogrid-reinforced counter-weight fill to increase the seismic stability of an existing earth dam, *Proc. 8th International Conference on Geosynthetics*, Yokohama, 2: 643-646.
- Min, Y., Leshchinsky, D., Ling, H.-I. and Kaliakin, V. N. (1995). Effects of sustained and repeated tensile loads on geogrid embedded in sand, *Geotechnical Testing Journal*, 18(2), 204-225.
- Morishima, H., Saruya, K. and Aizawa, F. (2005). Damage to soils structures of railway and their reconstruction, Special Issue on Lessons from the 2004 Niigata-ken Chu-Etsu Earthquake and Reconstruction, *Foundation Engineering and Equipment (Kiso-ko)*, October, 78-83 (in Japanese).
- Onodera, S., Fukuda, N. and Nakane, A. (2004). Long-term behavior of geogrid reinforced soil walls, *Proc. of the 3rd Asian Regional Conference on Geosynthetics (GeoAsia 2004)*, Seoul, 255-9-264.
- Railway Technical Research Institute (1999). Seismic design standard for railway structures. *Maruzen*, 47 and 89-90 (in Japanese).
- Railway Technical Research Institute (2007). Design standard for railway earth structures. *Maruzen*, 257 (in Japanese).
- Seida, T., Kawaharazono, M., Tobisu, Y., Tatsuoka, F. and Hirakawa, D. (2007). Strength and deformation characteristics of compacted diluvial sandy soil in drained plane strain compression, *Proc. 42th National Conference on Geotechnical Engineering, the JGS, Nagoya*, 359-360 (in Japanese).
- Seida, T., Tatsuoka, F. and Hirakawa, D. (2008). Deformation and strengths characteristics of highly compacted Inagi sand by drained plane strain compression test, *Proc. 43th National Conference on Geotechnical Engineering, the JGS, Hiroshima* (in Japanese).
- Shinoda, M. and Bathurst, R. J. (2004a). Lateral and axial deformation of PP, HDPE and PET geogrids under tensile load", *Geotextiles and Geomembranes*, 22: 205-222.
- Shinoda, M. and Bathurst, R.J., (2004b). Strain measurement of geogrids using a video-extensometer technique, *Geotechnical Testing Journal*, 27(5), 456-463.
- Shibuya, S., Kawaguchi, T. and Chae, J. (2007). Failure of reinforced earth as attached by typhoon No. 23 2004, *Soils and Foundations*, 47(1), 153-160.
- Takagi H., Sugimoto T., Nakamura Y., Kawahata S., Funada H., Yoshida T., Ito S. and Tatta N. (2007). Application of reinforced soil wall to high embankment in Mt. Fuji Shizuoka Airport, Part II: Earthwork, *Proc. of the 42nd Japan National Conference on Geotechnical Engineering, Nagoya*, No.803: 1601-1602 (in Japanese).
- Tatsuoka F. (1993). Roles of facing rigidity in soil reinforcing, Keynote Lecture, *Proc. Int. Sym. on Earth Reinforcement Practice, IS Kyushu '92* (Ochiai et al., eds), Balkema, 2: 831-870.
- Tatsuoka, F., Tateyama, M. and Koseki, J. (1996). Performance of soil retaining walls for railway embankments, *Soils and Foundations, Special Issue for the 1995 Hyogoken-Nambu Earthquake, Soils and Foundations*, 311-324.
- Tatsuoka, F., Koseki, J. and Tateyama, M. (1997a). Performance of Earth Reinforcement Structures during the Great Hanshin Earthquake, *Special Lecture, Proc. Int. Sym. on Earth Reinforcement, IS Kyushu '96*

- (Ochiai et al., eds), *Balkema*, 2: 973-1008.
- Tatsuoka, F., Tateyama, M., Uchimura, T. and Koseki, J. (1997b). Geosynthetics-reinforced soil retaining walls as important permanent structures, 1996-1997 Mercer Lecture, *Geosynthetics International*, 4(2), 81-136.
- Tatsuoka, F., Koseki, J., Tateyama, M., Munaf, Y. and Horii, N. (1998). Seismic stability against high seismic loads of geosynthetic-reinforced soil retaining structures, Keynote Lecture, *Proc. of the 6th Int. Conf. on Geosynthetics*, Atlanta, 1: 103-142.
- Tatsuoka, F., Santucci de Magistris, F., Hayano, K., Momoya, Y. and Koseki, J. (2000). Some new aspects of time effects on the stress-strain behaviour of stiff geomaterials”, Keynote Lecture, *The Geotechnics of Hard Soils – Soft Rocks, Proc. of 2nd Int. Conf. on Hard Soils and Soft Rocks*, Napoli, 1998 (Evangelista and Picarelli eds.), *Balkema*, 2: 1285-1371.
- Tatsuoka, F., Uchimura, T., Hayano, K., Di Benedetto, H., Koseki, J. and Siddiquee, M.S.A. (2001). Time-dependent deformation characteristics of stiff geomaterials in engineering practice, Theme Lecture, *Proc. of the 2nd Int. Conf. on Pre-failure Deformation Characteristics of Geomaterials*, IS Torino '99, *Balkema* (Jamiolkowski et al., eds.), 2: 1161-1262.
- Tatsuoka, F., Ishihara, M., Di Benedetto, H. and Kuwano, R. (2002). Time-dependent shear deformation characteristics of geomaterials and their simulation, *Soils and Foundations*, 42(2), 103-129.
- Tatsuoka, F. (2004). Effects of viscous properties and ageing on the stress-strain behaviour of geomaterials.” *Geomechanics- Testing, Modeling and Simulation, Proc. of the GI-JGS workshop*, Boston, ASCE Geotechnical Special Publication GSP No. 143, Yamamuro & Koseki (eds.), 1-60.
- Tatsuoka, F., Hirakawa, D., Shinoda, M., Kongkitkul, W. and Uchimura, T. (2004). An old but new issue; viscous properties of polymer geosynthetic reinforcement and geosynthetic-reinforced soil structures”, Keynote Lecture, *Proc. of the 3rd Asian Regional Conference on Geosynthetics (GeoAsia 2004)*, Seoul, 2: 29-77.
- Tatsuoka, F., Kongkitkul, W. and Hirakawa, D. (2006). Viscous property and time-dependent degradation of geosynthetic reinforcement, *Proc. of the 8th International Conference on Geosynthetics, Yokohama, Japan* (Kuwano & Koseki, eds.), 4: 1587-1590.
- Tatsuoka, F. (2007). Inelastic deformation characteristics of geomaterial”, Special Lecture, *Soil Stress-Strain Behavior: Measurement, Modeling and Analysis, Proc. of Geotechnical Symposium in Roma*, March 16 & 17, 2006 (Ling et al., eds.), Springer, 1-108.
- Tatsuoka, F., Koseki, J., Tateyama, M. and Hirakawa, D. (2007a). Recent developments of geosynthetic-reinforced soil structures to survive strong earthquakes, *Proc. of the 4th International Conference on Earthquake Geotechnical Engineering*, June 25-28, 2007, Thessaloniki, Greece, No.W1-1003, 256-273.
- Tatsuoka, F., Tateyama, M., Mohri, Y. and Matsushima, K. (2007b). Remedial treatment of soil structures using geosynthetic-reinforcing technology, *Geotextiles and Geomembranes*, 25(4-5), 204-220.
- Tatsuoka, F., Hirakawa, D., Nojiri, M. and Aizawa, H., Tateyama, M. and Watanabe, K. (2007c). A new type integral bridge comprising of geosynthetic-reinforced soil walls, *Proc. of 5th Int. Sym. on Earth Reinforcement* (IS Kyushu 2007) (Ochiai et al., eds.), 803-809.
- Tatsuoka, F., Di Benedetto, H., Enomoto, T., Kawabe, S. and Kongkitkul, W. (2008a). Various viscosity types of geomaterials in shear and their general expression, *Soils and Foundations*, 48(1), 41-60.
- Tatsuoka, F., Hirakawa, D., Nojiri, M., Aizawa, H., Tateyama, M. and Watanabe, K. (2008b). Integral Bridge with Geosynthetic-Reinforced Backfill, *the First Pan American Geosynthetics Conference & Exhibition*, Cancun, Mexico, 1199-1208.
- Tatsuoka, F., Hirakawa, D., Aizawa, H., Nishikiori, H., Soma, R. and Sonoda, Y. (2008c). Importance of strong connection between geosynthetic reinforcement and facing for GRS integral bridge, *Proc. 4th GeoSyntheticsAsia*, Shanghai.
- Tatsuoka, F. (2008). Design shear strength and compaction control of backfill - a current wide and deep gap between Industry and Academia –, *Panel discussions for Industry and Academia Session, Proc. 13th Asian Regional Conference on SMGE*, Kolkata, 2: (to appear).
- Thornton, J. S., Paulson, J. N. and Sandri, D. (1998). The stepped isothermal method for time-temperature superposition and its application to creep data on polyester yarn”, *Proc. of the 6th International Conference on Geosynthetics*, Atlanta, USA, .2: 699-706.
- Tobisu, Y., Kawaharazono, M., Tatsuoka, F. and Hirakawa, D. (2008). Effects of compaction conditions on drain strength and deformation of unsaturated gravelly soil, *Proc. 43th National Conference on Geotechnical Symposium, the JGS, Hiroshima* (in Japanese)..
- Voskamp, W., Van Vliet, F. and Retzlaff, J. (2001). Residual strength of PET after more than 12 years creep loading, *Landmarks in Earth Reinforcement; Proc. of the International Symposium on Earth Reinforcement* (Ochiai et al., eds.), *Balkema*, 1: 165-170.
- Zornberg, J. G. and Kavazanjian, E, Jr. (2002). Closures on: Prediction of the performance of a geogrid-reinforced slope founded on solid waste, *Soils and Foundations*, 42(5), 129-130.
- Zornberg, J. G., Byler, B. R. and Knudsen, J. W. (2004). Creep of geotextiles using time-temperature superposition methods, *Journal of Geotechnical and Geoenvironmental Engineering*, 130(11), 1158-1168.